Research Square

Preprints are preliminary reports that have not undergone peer review.
They should not be considered conclusive, used to inform clinical practice,
or referenced by the media as validated information.

Limb salvage in a Ukrainian soldier with Klebsiella pneumoniae osteomyelitis: phage-antibiotic therapy despite anti-phage antibodies

Karlis Racenis

karlis.racenis@rsu.lv

Riga Stradins University https://orcid.org/0000-0001-7123-4048

Renate Apse

Riga Stradins University

Lise Berentsen

Riga Stradins University

Sandis Maurins

Riga Stradins University

Dace Eglite

Riga Stradins University

Nikita Zrelovs

Riga Stradins University

Krystyna Dąbrowska

Hirszfeld Institute of Immunology and Experimental Therapy, Weigla 12, Wrocław, Poland

Zuzanna Kazmierczak

Hirszfeld Institute of Immunology and Experimental Therapy, Polish Academy of Sciences

Roberto Sierra

University of Geneva https://orcid.org/0000-0002-8657-1781

Diego Andrey

University of Geneva

Léna Falconnet

University of Geneva

Mélanie Roch

University of Geneva https://orcid.org/0000-0001-6485-8434

Nikola Brauca

Riga Stradins University

Laima Sevastjanova

Riga Stradins University

Kitija Straumane

Riga Stradins University
Juta Kroica
Riga Stradins University
Monta Madelane
Riga East Clinical University Hospital
Dace Rudzite
Riga East Clinical University Hospital
Jevgenijs Movcans
Riga East Clinical University Hospital
Konstantins Plotnikovs
Riga East Clinical University Hospital
Anda Vilmane
Riga Stradins University
Marika Kalnina
ARS
Izabela Rybicka
Hirszfeld Institute of Immunology and Experimental Therapy, Polish Academy of Sciences
Aleksandra Wilczak
Hirszfeld Institute of Immunology and Experimental Therapy, Polish Academy of Sciences

---

Article

Keywords: War-related infection; chronic osteomyelitis; bacteriophage-antibiotic therapy; antibiotic-resistance; immunology; case report

Posted Date: November 12th, 2026

DOI: https://doi.org/10.21203/rs.3.rs-11661571/v1

License: This work is licensed under a Creative Commons Attribution 4.0 International License.
Read Full License

Additional Declarations: There is **NO** Competing Interest.

Limb salvage in a Ukrainian soldier with *Klebsiella pneumoniae* osteomyelitis: phage-antibiotic therapy despite anti-phage antibodies

Authors:

Renate Ruta Apse*, Lise Berentsen*, Sandis Maurins, Dace Eglite, Nikita Zrelovs, Krystyna Dabrowska, Zuzanna Maria Kazmierczak, Roberto Sierra, Diego O. Andrey, Léna Falconnet, Mélanie Roch, Nikola Brauca, Laima Sevastjanova, Kitija Straumane, Juta Kroica, Monta Madelane, Dace Rudzite, Jevgenijs Movcans, Konstantins Plotnikovs, Anda Vilmane, Marika Kalnina, Izabela Rybicka, Aleksandra Wilczak, Karlis Racenis**.

*These authors contributed equally: Renate Ruta Apse, Lise Berentsen
** Corresponding author: Karlis Racenis (Karlis.Racenis@rsu.lv)

Abstract

Chronic osteomyelitis caused by antibiotic-resistant bacteria represents a major therapeutic challenge, particularly in patients with war-related traumatic injuries, where prolonged hospitalization and extensive tissue damage increase the emergence of resistant pathogens. Treatment of *Klebsiella pneumoniae* poses distinctive challenges in this context, as phage-host interactions are predominantly determined by the pathogen's hypervariable polysaccharide capsule, which restricts phage activity to strains with compatible capsular receptor structures and necessitates highly individualized phage selection. However, clinical evidence remains limited, and detailed description of immunological response to treatment is still scarce. We report a case of chronic femur osteomyelitis caused by multidrug-resistant (MDR) *K. pneumoniae* in a Ukrainian war-trauma patient, successfully treated with a multimodal informed selected bacteriophage regimen combining systemic intravenous, local intraoperative, and continuous intramedullary administration alongside targeted antibiotic therapy.

Serial serological and cytokine profiling were performed before, during, and after the treatment to characterize the immunological response. Immunological profiling showed consistent antigen recognition for both phages used. Elevated baseline serum IgA titres specific to one phage demonstrated prior mucosal exposure to this or a structurally similar phage. Notably, serum-mediated phage neutralization exceeded 99% by day 11 of treatment yet did not impair therapeutic effectiveness.

This case demonstrates that multimodal phage delivery combined with antibiotic treatment can lead to infection resolution in MDR osteomyelitis despite a robust anti-phage immune response.

Keywords: War-related infection; chronic osteomyelitis; bacteriophage-antibiotic therapy; antibiotic-resistance; immunology; case report

Introduction

War-related traumatic injuries, including those caused by explosions and gunshot wounds, frequently result in complex open fractures with extensive soft-tissue damage, predisposing patients to chronic bone and soft-tissue infections[1,2]. Russia's full-scale invasion of Ukraine has led to a surge of patients with musculoskeletal injuries requiring prolonged and complex medical care[3,4]. These injuries are often complicated by colonization or infection of multidrug-resistant (MDR) microorganisms, reflecting a combination of environmental contamination, repeated healthcare exposures, prolonged antibiotic use, and extended hospitalization[5–7].

Gram-negative pathogens such as *Klebsiella pneumoniae* have become clinically important because of their capacity to acquire and disseminate antimicrobial resistance determinants[8,9]. Chronic osteomyelitis caused by MDR microorganisms is difficult to eradicate because of the limited penetration of many antimicrobials into bone tissue, the need for prolonged treatment courses, and ability of bacteria to establish biofilms on implanted hardware[10,11].

Bacteriophage (phage) therapy - the use of bacterial viruses to selectively lyse target pathogens - is particularly of interest in this context due to their capacity for self-amplification at the site of infection, activity against biofilm-associated bacteria, and potential synergy with antibiotics [12–14].

Systematic reviews suggest that phage therapy may represent a promising adjuvant strategy for bone and joint infections. Genèviere et al. (2021) reported that 71% of 52 published treatment episodes with concomitant antibiotic therapy was administered in 79% of cases[15]. Similarly, Suh et al. (2023) identified favourable outcomes in 87% of 33 reported cases involving bone and joint infections[16]. In *Klebsiella*, K-antigens of the capsule are the main attachment point for phages, as the capsule masks other surface structures, such as LPS. *Klebsiella* capsules are known to have an extensive variation, with 77 distinct types with more than 160 capsular loci having been described, with the six most common types accounting for less than 40% of the clinical isolates[17,18]. This diversity, together with the capability of *K. pneumoniae* to lose capsule production, makes phage therapy difficult[19–21].

The therapeutic success of phages depends not solely on the lytic activity of the administered phages, but also on the host's immune response. Phage virions can act as T-dependent antigens, inducing mature and highly specific IgG antibodies that can be devastating to the

phage and are linked to the development of immunological memory[22,23]. Phage-specific antibodies can directly neutralize phages if they target proteins involved in bacterial recognition. However, antibodies targeting other virion components may contribute to phage clearance through innate mechanisms, including immunophagocytosis and activation of the classical complement pathway[22,23]. Consequently, anti-phage immune responses have the potential to influence phage persistence and therapeutic efficacy, although their clinical significance remains poorly understood[24–26].

Anti-phage immunity may have direct implication for the success of phage therapy. Firstly, pre-existing antibodies can be generated through natural exposure to phages in the environment and the human phageome. Consequently, individuals who have never received phage therapy are not necessarily immunologically naïve to therapeutic phages, particularly when therapeutic phages share antigenic similarities with those naturally present in the environment and the human phageome[22,27,28]. Although such antibodies could theoretically reduce the effectiveness of phage therapy, robust evidence supporting this hypothesis remains limited. Secondly, immune responses can be elicited by therapeutic phages during treatment. While such responses have been documented, the extent to which they compromise therapeutic efficacy appears to be limited. Reports suggest the existence of a therapeutic window between first exposure to the phage and the development of phage-specific neutralizing antibodies that may be sufficient to achieve infection control[29–31].

Beyond humoral immunity, phages may elicit cytokine responses that vary depending on the phage, bacteria target, and host environment[32]. In Gram-negative infections, phage-mediated bacterial lysis may additionally promote the release of endotoxins, potentially amplifying pro-inflammatory cytokine responses[32,33].

Here, we report the treatment of chronic osteomyelitis caused by MDR *K. pneumoniae* in a Ukrainian soldier with a war-related fracture. This case report highlights two novel aspects that remain underrepresented in the phage therapy literature. First, phage therapy was delivered through a multimodal approach combining systemic intravenous administration with local intraoperative application and continuous intramedullary infusion alongside targeted antibiotic therapy. Second, we performed a longitudinal immunological characterization of the host immune response.

Case presentation

A 42-year-old Ukrainian male was referred to Riga East Clinical University Hospital in November 2024 for the management of a war-related injury involving the right femur. On 27 September 2024, the patient had sustained blast injuries to all four extremities and the abdomen, which were initially managed in Ukraine, resulting in amputation of the right forearm, emergency laparotomy, and skin grafting of the lower-limb wounds. Of these, the

injury that remained unsolved was a distal-third femoral fracture associated with soft-tissue defect, which had been managed with wound revision and placement of an external fixation device (EFD). Upon admission into the hospital in Latvia, the patient was clinically stable, had no relevant comorbidities and reported no regular medication use.

Between December 2024 and February 2025, the patient underwent a series of surgical procedures as part of fracture management and subsequent infection control (Figure 1). Minimally invasive osteosynthesis with internal fixation was performed on 5 December 2024; however, the postoperative course was complicated by persistent wound discharge and failure of surgical wound to heal. Repeated microbiological cultures obtained from wound and bone samples consistently yielded carbapenem-resistant *K. pneumoniae*; the isolate was identified as a *K. pneumoniae* carbapenemase (KPC) producer (Supplementary Table 1). Subsequent interventions included debridement with placement of an EFD, insertion of an intra-soft tissue antibiotic perfusion (iSAP) system (14 December 2024), closure of the soft-tissue defect with parascapular flap (18 December 2024), soft-tissue revision (20 December 2024), removal of internal fixation hardware with debridement (2 January 2025), additional soft-tissue debridement with local irrigation (8 January 2025), and replacement of an EFD screw because of the pin-site infection (4 February 2025). Concurrent antimicrobial therapy consisted of colistin from 18 December 2024 to 11 March 2025 and local gentamicin administered through the iSAP system from 14 - 17 December 2024.

Despite the intensive surgical and antimicrobial management, the infection recurred in May 2025, presenting as a draining fistula above the right knee. Microbiological cultures again yielded KPC-producing *K. pneumoniae* as the causative pathogen. Inflammatory markers remained elevated, supporting the presence of ongoing active infection (Supplementary Figure 1). After surgery on 5 June 2025, antibiotic treatment was initiated with tigecycline (100 mg twice daily, i.v.) and colistin (3 MIU three times daily, i.v.), together with gentamicin administered continuously through an intramedullary catheter (60 mg, continuous infusion). Due to adverse side-effects (nausea, vomiting, and elevated serum creatinine), tigecycline and colistin were discontinued, and ceftazidime-avibactam was initiated on 27 June 2025 (2.5 g three times daily, i.v.).

Given the failure of prolonged conventional management, including continuous local intramedullary gentamicin infusions, the case was reviewed by a multidisciplinary team comprising specialists in infectious diseases, orthopaedic surgery, internal medicine with experience in phage therapy, and clinical microbiology. The team recommended repeat surgical debridement combined with adjunctive phage therapy because the infection involved both deep intramedullary and soft-tissue locations, the causative agent *K. pneumoniae* isolate remained MDR; and the retained EFD represented a potential nidus for

biofilm persistence, collectively reducing the likelihood of achieving durable infection control through conventional strategies alone. Phage therapy was administered under the magistral preparation framework, whereby a patient-specific phage preparation was compounded for individual therapeutic use in accordance with Article 37 of the Declaration of Helsinki[32]. Written informed consent for treatment and publication of this case report was obtained from the patient.

The phage treatment regimen was designed for 11 days considering the available phage preparation, the multimodal administration, and the possibility of host-mediated phage neutralization developing during therapy. Treatment was initiated on 4 July 2025 and comprised three complementary routes of administration:

1. *Systemic intravenous delivery.* A pre-established dual-phage combination (DPC) containing GPH19 and GPH164 with ratio 1:1 at a final concentration of 10^7 plaque-forming units per millilitre (PFU/mL) was administered through a central venous catheter at 10 mL/h for 7 hours daily (total 70 mL/day) in 0.9% NaCl. The first intravenous infusion was initiated at 9:37am (several hours before surgery), and no adverse effects were observed. Systemic i.v. administration continued daily for 11 consecutive days (from 11:00 to 18:00);
2. *Local intraoperative delivery.* During surgery, the wound site was pre-irrigated with 250mL 4.2% sodium bicarbonate solution, followed by irrigation with 45 mL of the GPH19/GPH164 DPC (10^7 PFU/mL). Subsequently, 15 mL of Defensive Antibacterial Coating (DAC) hydrogel impregnated with the same DPC (10^7 PFU/mL) was applied locally (Supplementary Figure 2 and 3). The suitability of DAC hydrogel as a phage carrier has been addressed in previous clinical reports[34], in which the gel did not measurably affect the lytic activity and titres remained stable for at least 6h[35,36];
3. *Continuous local intramedullary delivery.* Postoperatively, the DPC was infused continuously through an intramedullary catheter at 2.5 mL/h for 20 hours daily over 11 days.

Throughout the course of phage therapy, ceftazidime-avibactam was administered i.v. at a dose of 2.5 g three times daily (6:00am; 2:00pm; 10:00pm), and local gentamicin was co-administered with phages continuously through the intramedullary catheter at 2.5 mL/h (60 mg per 20 hours). Notably, phages were administered via a dedicated central venous catheter with no other medications co-infused, antibiotics were administered through a separate peripheral venous catheter. Continuous local intramedullary gentamicin infusion had been administered during an earlier treatment period without achieving sustained infection control (Figure 1).

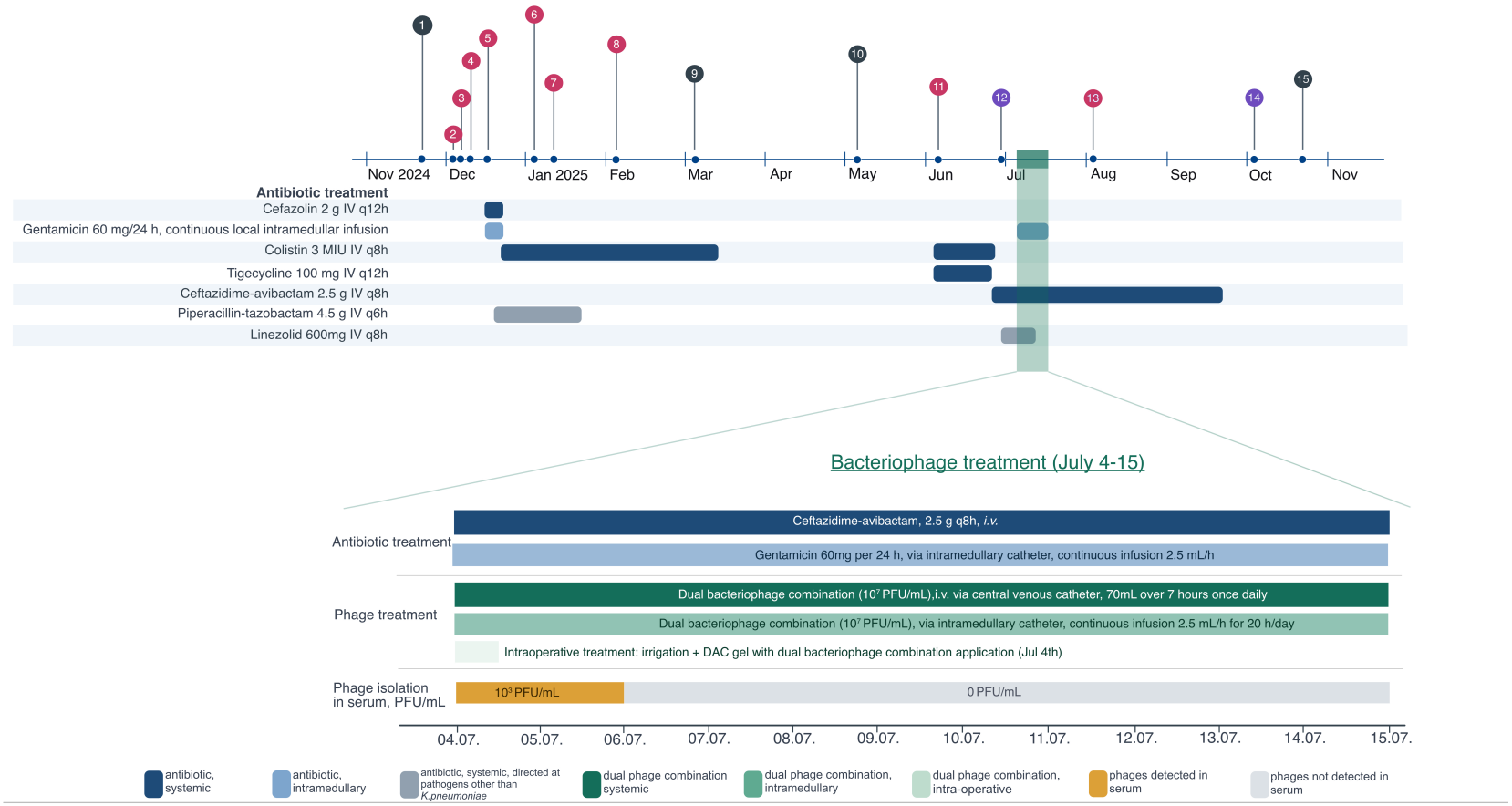


Figure 1. Timeline of the patient's clinical course, antimicrobial treatment, and phage therapy. The upper panel summarized the major clinical events from admission (November 2024) to discharge from hospital (October 2025) and antibiotic treatment. The lower panel summarizes an expanded view of the active phage treatment period (4-15 July 2025), showing concomitant antimicrobial therapy, multimodal administration of GPH19/GPH164 DPC, and the detection of circulating phages in serum.

Clinical course and treatment outcomes

Following initiation of combined phage and antibiotic treatment, inflammatory markers declined over time (Supplementary Figure 1). CRP reached its lowest values during the entire hospitalization period (3.8 mg/L) 10 days after treatment initiation, while the leukocyte count normalized after two weeks. No adverse effects related to phage treatment were recorded during the treatment. At follow-up samples obtained on 4 August 2025 from the patient wound, showed no growth of *K. pneumoniae* or any other pathogen.

Whole-body [18F]FDG PET/CT at baseline demonstrated heterogeneous hypermetabolism in the right femur corresponding to a non-union fracture complicated by chronic osteomyelitis. Metabolic activity was most pronounced along the external fixation hardware, including the proximal screw and fracture site, as well as around distal screws adjacent to the knee joint. Diffuse low-grade FDG uptake was also observed in the surrounding soft tissues of the mid and distal thigh, consistent with post-surgical inflammatory changes (Supplementary Figure 4 and 5). In this clinical context, persistent infection could not be excluded and was considered likely. No evidence of distant infectious dissemination was identified.

At the 4-month follow-up after phage therapy, PET/CT demonstrated a favourable metabolic response, with a marked reduction in FDG uptake across all previously involved regions. Residual focal uptake persisted along the fixation hardware, most pronounced at the distal screws (SUVmax up to 4.7), likely reflecting a combination of post-surgical inflammation and reparative processes (Supplementary Figure 4 and 5). Diffuse low-grade uptake in adjacent soft tissues remained stable. No new hypermetabolic lesions or evidence of systemic infectious spread were detected. Notably, despite residual FDG uptake, the patient showed sustained clinical improvement without evidence of recurrent infection. These findings highlight the potential of FDG PET/CT to monitor treatment response in complex osteomyelitis, while underscoring the importance of clinical correlation in interpreting residual metabolic activity.

Following initial rehabilitation, the patient was discharged and subsequently returned to Ukraine for continued rehabilitation (Figure 2). Functional recovery included progressive weight-bearing capacity. The patient has been followed for 15 months since the initiation of phage therapy with clinical monitoring being held both in Latvia and Ukraine. At the clinical assessment in June 2026, there was no clinical evidence of infection recurrence, and complete bone healing was confirmed both clinically and radiologically. Following the removal of EFD, the patient regained independent ambulation with a hinged knee orthosis (Figure 2). At the most recent follow-up contact with the patient in October 2026, no clinical signs of infection were reported.

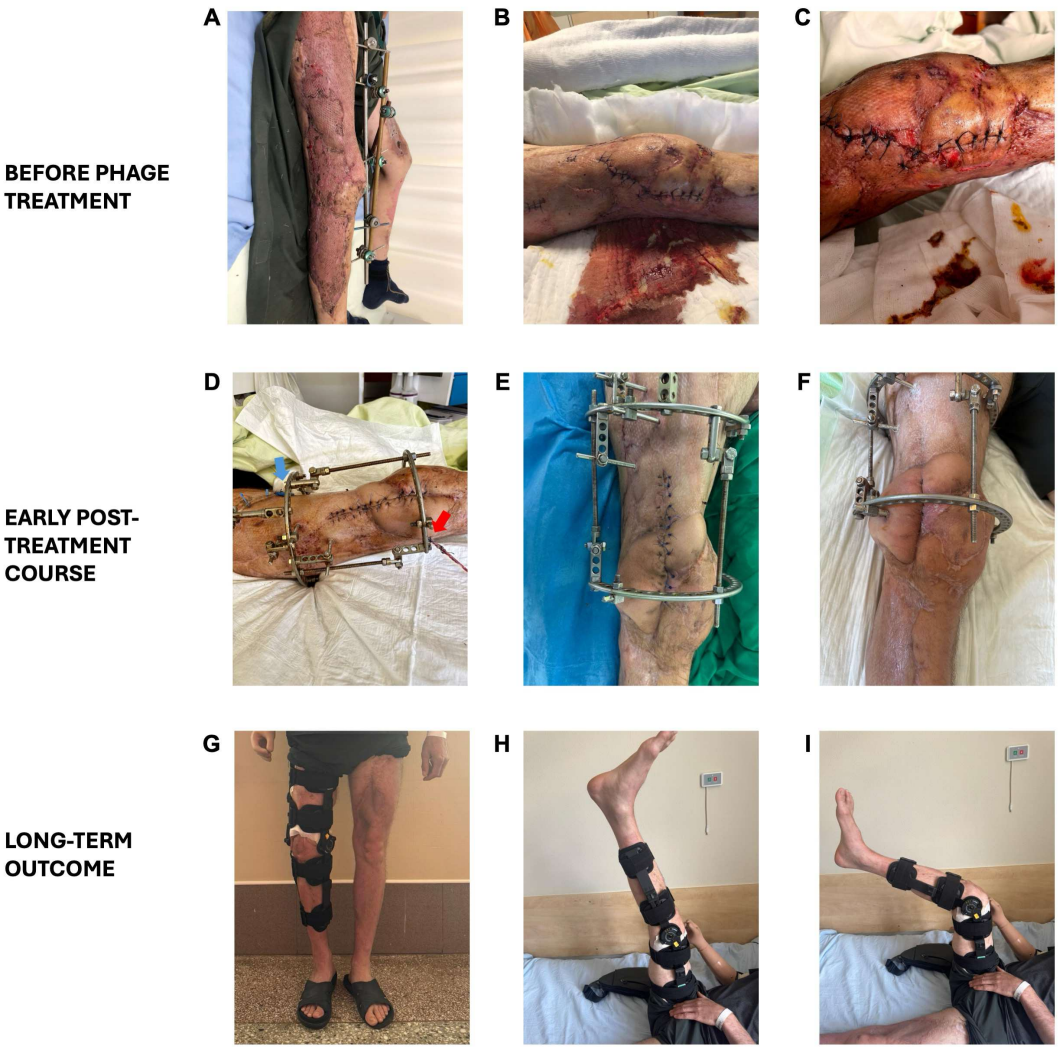


Figure 2. Clinical appearance of the patient's right leg throughout hospitalization. Before phage treatment: at the moment of hospitalisation (A) November 2024; wound at initial presentation when infection was first identified (B and C) December 2024.
Clinical appearance of the patient's right leg after phage treatment July 2025 (D – blue arrow (entry site of the intramedullary catheter), red arrow (exit site of the catheter)), August 2025 (E), October 2025 (F) and June 2026 (G, H, I), showing no clinical signs of infection. Serial radiographs are provided in Supplementary Figure 6.

RESULTS

Bacteria and phage characterization

Genomic characterization of the infecting isolate using Kleborate assigned a resistance score of 2 and a virulence score of 0, consistent with a multidrug-resistant but non-hypervirulent phenotype. Capsule typing using Kaptive identified the KL107 capsule locus. Given the susceptibility of the isolate to phages from the GENeva PHage (GENPH) Collection, two lytic

phages, GPH19 and GPH164, were selected for therapeutic use. This DPC had previously been established against KL107-producing ST258 and ST512 *K. pneumoniae* (for further genomic characterisation see Supplementary Note 1) through screening of the GENPH Collection against paired encapsulated and non-encapsulated derivatives, revealing complementary activity profiles against distinct bacterial subpopulations. GPH19 belongs to the genus Przondovirus, and targets KL107-encapsulated isolates, but shows reduced activity against capsule-deficient derivatives. In contrast, GPH164 belongs to the genus Teetrevirus and infects these non-encapsulated derivatives. Combining two phages targeting different bacterial phenotypes therefore provides complementary selective pressure that can reduce or delay resistant outgrowth compared with either phage alone[19,37]. Both phages belong to the Autotranscriptaviridae family and exhibit podoviral morphology and lack identifiable toxin, lysogeny-associated, or antibiotic resistance genes (Supplementary Figure 7).

Antimicrobial susceptibility testing, interpreted according to EUCAST version 15.0 breakpoints, demonstrated an MDR phenotype (Table 1), with resistance to most β-lactams, fluoroquinolones, aminoglycosides, and trimethoprim-sulfamethoxazole, while retaining susceptibility to ceftazidime-avibactam, gentamicin, colistin, and tigecycline. Phage titres were determined on both the original host and the patient isolate. GPH19 reached a titre on its original host of 5.45×10^9 PFU/mL, whereas GPH164 reached 1.67×10^8 PFU/mL. When tested against the patient's isolate, GPH19 demonstrated confluent lysis (++++) with an efficiency of plating (EOP) of 0.99, indicating near-equivalent infectivity compared with its propagation host. In contrast, GPH164 produced only partial lysis (++) and exhibited a markedly reduced EOP of 1.6×10^{-4} (Table 1). Although these findings indicated substantial differences in activity against dominant baseline clinical isolate, the GPH19/GPH164 DPC had previously been selected based on complementary activity profiles against encapsulated and non-encapsulated ST258 and ST512 derivatives.

Biofilm formation was assessed for the patient isolate over a 6-48 h time course using the crystal violet assay. Patient's isolate produced biofilm biomass, but slightly less than the positive control (Supplementary Figure 8).

Table 1. Antimicrobial and phage susceptibility profile of the patient's *K. pneumoniae* isolate. *Susceptibility interpreted per EUCAST breakpoints (version 15.0). S, susceptible; R, resistant; I, susceptible, increased exposure; MIC, minimum inhibitory concentration; EOP, efficiency of plating; ++++, confluent lysis; ++, partial lysis.*

Antimicrobial agent	Susceptibility
Amoxicillin–clavulanate (p/os)	**R**
Amoxicillin–clavulanate (i/v)	**R**

Ampicillin	**R**
Piperacillin	**R**
Piperacillin-Tazobactam	**R**
Cefepime	**R**
Ceftriaxone	**R**
Ceftazidime-Avibactam	S
Ceftolozane-Tazobactam	**R**
Imipenem	**R**
Meropenem	I
Aztreonam	**R**
Amikacin	**R**
Gentamicin	S
Tigecycline	MIC ≤ 0,25
Ciprofloxacin	**R**
Levofloxacin	**R**
Colistin	S
Trimethoprim-sulfamethoxazole	**R**
Phage	**Lytic Activity (EOP)**
GPH19	++++ (EOP = 0.99)
GPH164	++ (EOP = 0.00016)

Phage-antibiotic interactions enhance bacterial growth suppression

Minimum inhibitory concentrations were determined for tigecycline, gentamicin, colistin, and ceftazidime-avibactam antibiotics against the patient's *K. pneumoniae* isolate, both alone and in combination with the DPC (10^7 PFU/mL) at MOI 1 (Supplementary Figure 9). At antibiotic concentrations that permitted bacterial growth during monotherapy, the addition of the DPC resulted in near-complete growth inhibition ($OD_{600} < 0.1$) across all four antibiotics tested. Combination treatment enhanced bacterial growth suppression by three to four twofold dilutions compared with antibiotics alone.

Phage antibacterial activity and multiplicity of infection (MOI) dependence

The DPC of GPH19 and GPH164 was evaluated against the patient-derived clinical isolate RSU-KP-Osteomyelitis1. In liquid killing assays, GPH19 alone delayed bacterial growth but was consistently followed by resistant outgrowth, while GPH164 alone did not affect bacterial

growth. In contrast, when combined, the GPH19/GPH164 DPC showed a clear synergistic effect, resulting in the most sustained growth suppression, preventing detectable growth for approximately 18 h at MOI 1 (Figure 3). The same overall pattern was also observed at MOI 0.1, although inhibition was less sustained (Supplementary Figures 10 and 11). Pre-established dual-phage combinations against high-risk lineages, such as the ST512-KL107, therefore represent a promising strategy to improve antibacterial activity and delay resistant outgrowth[38].

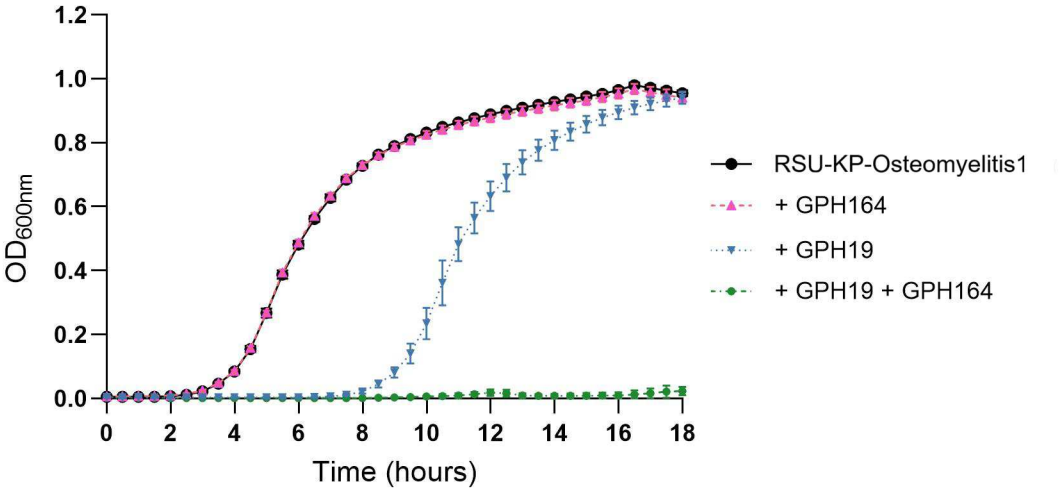


Figure 3. Growth suppression by individual phages and the DPC against the patient-derived *K. pneumoniae* isolate RSU-KP-Osteomyelitis1. Bacteria were cultured in cation-adjusted Mueller–Hinton broth without phage (black circles), with GPH164 (pink triangles), with GPH19 (blue triangle), or with the DPC (green circle) at MOI 1. OD600 was measured every 30 min for 18 h. Data are shown as mean ± SD of three biological replicates.

Phage-specific antibody responses during therapy

To provide a population context for the patient's pre-existing antibody reactivity to GPH19 and GPH164, serum IgM, IgG, and IgA levels were measured by ELISA one day before treatment and compared with the corresponding levels in 50 healthy donors with no history of phage therapy. The patient's GPH19- and GPH164-specific IgG values exceeded those in 37/50 (74%) and 35/50 (70%) control samples, respectively, although absolute ELISA values were low for both phages (Figure 4). GPH19-specific IgM was low and IgA was undetectable. By contrast, both isotypes were detectable against GPH164, and the patient's GPH164-specific IgA exceeded that in 49/50 control samples (Figure 4). Thus, pretreatment serum showed clear reactivity to GPH164, most notably a strong IgA response, whereas reactivity to GPH19 was weak or undetectable.

Phage-specific antibody profiles changed during and after therapy (Figure 5). GPH19-specific IgM increased during the first week, peaked around days 8–9, and subsequently declined. GPH19-specific IgA remained undetectable, whereas IgG increased gradually and reached its highest level at late follow-up (day 90). GPH164-specific antibodies showed broader pretreatment reactivity. IgM increased rapidly after treatment initiation, peaked around days 5–6, and then declined. IgA remained elevated throughout follow-up but showed no clear treatment-associated increase. GPH164-specific IgG increased gradually during treatment, followed by a more pronounced rise at late follow-up (days 21, 28, 90). These observations suggest that, despite detectable pretreatment reactivity to GPH164, therapeutic exposure elicited a phage-specific antibody response with kinetics resembling those of a primary humoral response in both phages.

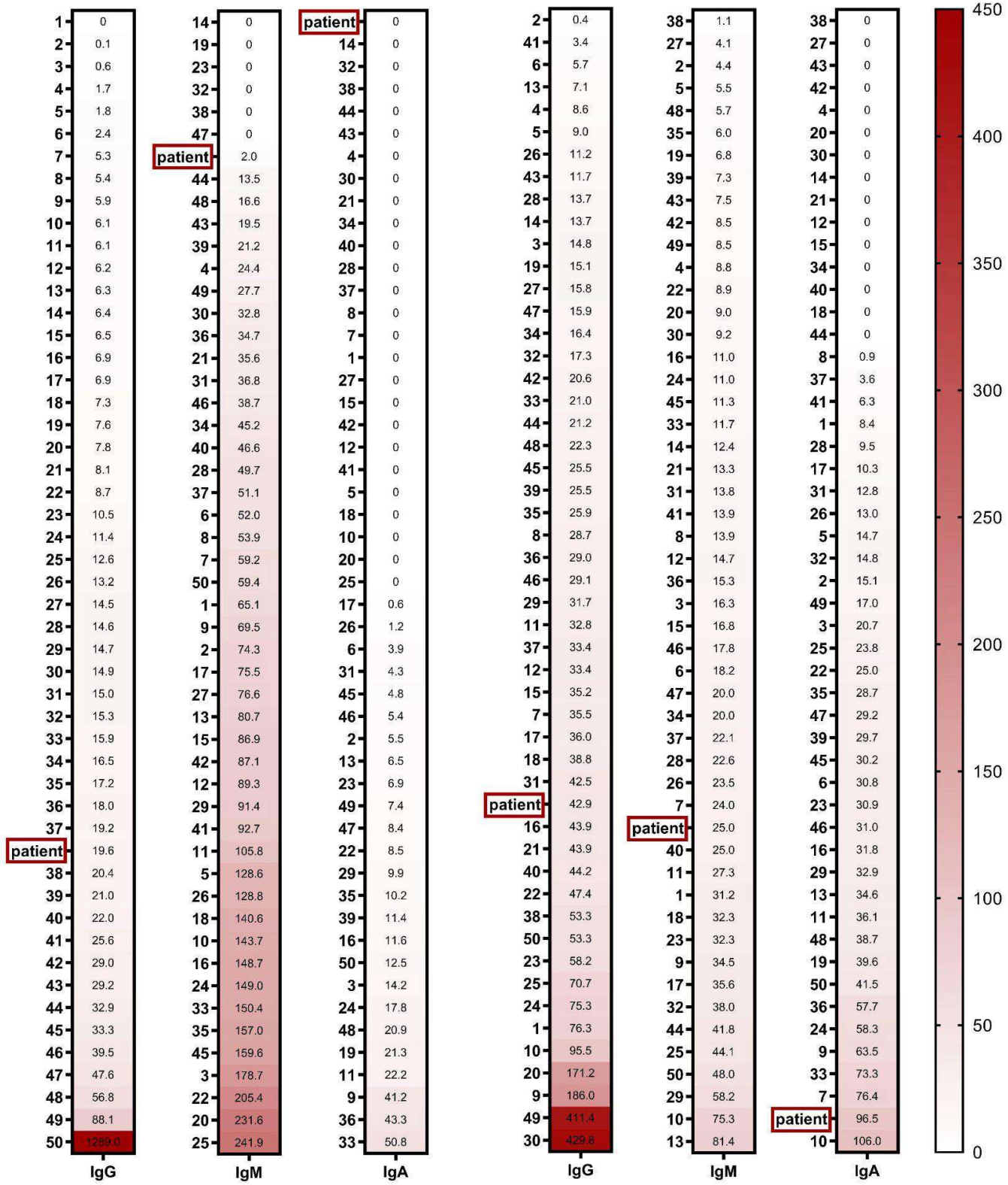

A.
GPH19
B.
GPH164
IgG
IgM
IgA
patient
450
400
350
300
250
200
150
100
50
0

Figure 4. Pretreatment phage-specific antibody reactivity in the patient and healthy control donors. Serum IgG, IgM, and IgA against GPH19 (A) and GPH164 (B) were quantified by ELISA in the patient on day −1 and in 50 healthy donors with no history of phage therapy. Cell values and colour intensity represent normalized ELISA units calculated as described by Miura et al.[39]. Control donors are ordered by increasing antibody reactivity within each panel, and the patient's position is indicated.

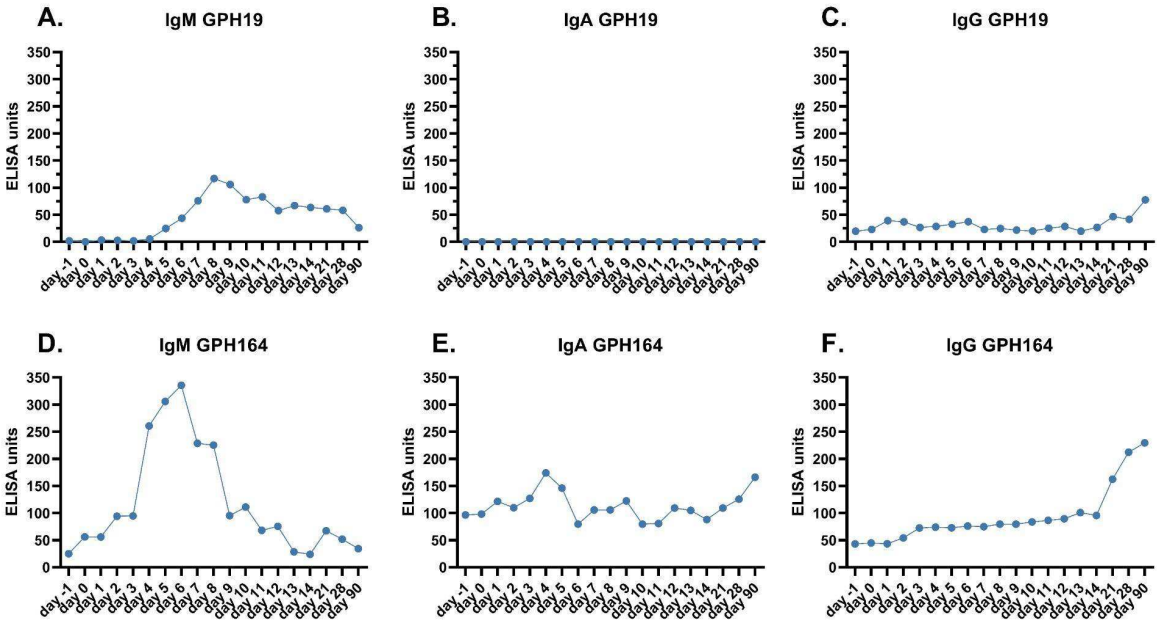


Figure 5. Kinetics of phage-specific antibody responses in the patient during and after phage therapy. Serum IgM, IgA, and IgG against GPH19 (A–C) and GPH164 (D–F) were quantified by ELISA at serial time points from day −1 to day 90. ELISA units were calculated as described by Miura et al.[39].

Serum-mediated phage neutralization

Despite detectable pretreatment antibody binding, baseline serum showed limited neutralizing activity against either therapeutic phage (Figure 6). Native pretreatment serum showed minimal, if any, neutralizing activity against GPH19, whereas its effect on GPH164 was negligible. Administered phages were initially detectable in blood at low but measurable titres (approximately 10^3 PFU/mL) but only on day 1 and 2 after treatment initiation; from day 3 onward, no active phages were recovered from blood.

Ex vivo assays showed that serum neutralizing activity against GPH19 developed rapidly during therapy. On day 6, native serum at a 1:10 dilution reduced infective phage titre by approximately three orders of magnitude (99.9%) relative to the control. By day 11, near-

complete neutralization was observed at 1:10 and 1:100 dilutions, whereas neutralizing activity was weak at 1:1000. To assess the potential contribution of serum complement, neutralization was compared between native and heat-inactivated serum. Heat inactivation reduced neutralizing activity under some conditions, most clearly at a 1:10 dilution on day 6, but did not abolish it. By day 11, strong neutralization was retained in heat-inactivated serum at 1:10 and 1:100 dilutions, showing that the effect was not entirely heat-sensitive.

Neutralization of GPH164 developed more gradually. At a 1:10 dilution, native serum reduced infective phage titre by less than one order of magnitude on day 6 (approximately 50%), by two orders of magnitude on day 11 (99.0%), and by more than three orders of magnitude on day 90 (99.96%). Neutralization was weaker at a 1:100 dilution but increased over time, reaching a reduction of nearly one order of magnitude (87.9%) by day 90. No clear evidence of neutralization was observed at 1:1000.

Heat-inactivated serum showed substantially reduced neutralizing activity against GPH164. At 1:10, infective phage titres were reduced by only approximately 1.7 orders of magnitude on day 11 (97.9%) and 1.9 orders of magnitude on day 90 (98.7%). At 1:100, however, heat inactivation had no consistent directional effect across time points. Overall, the dominant effect of heat inactivation was again attenuation, rather than complete loss, of neutralizing activity.

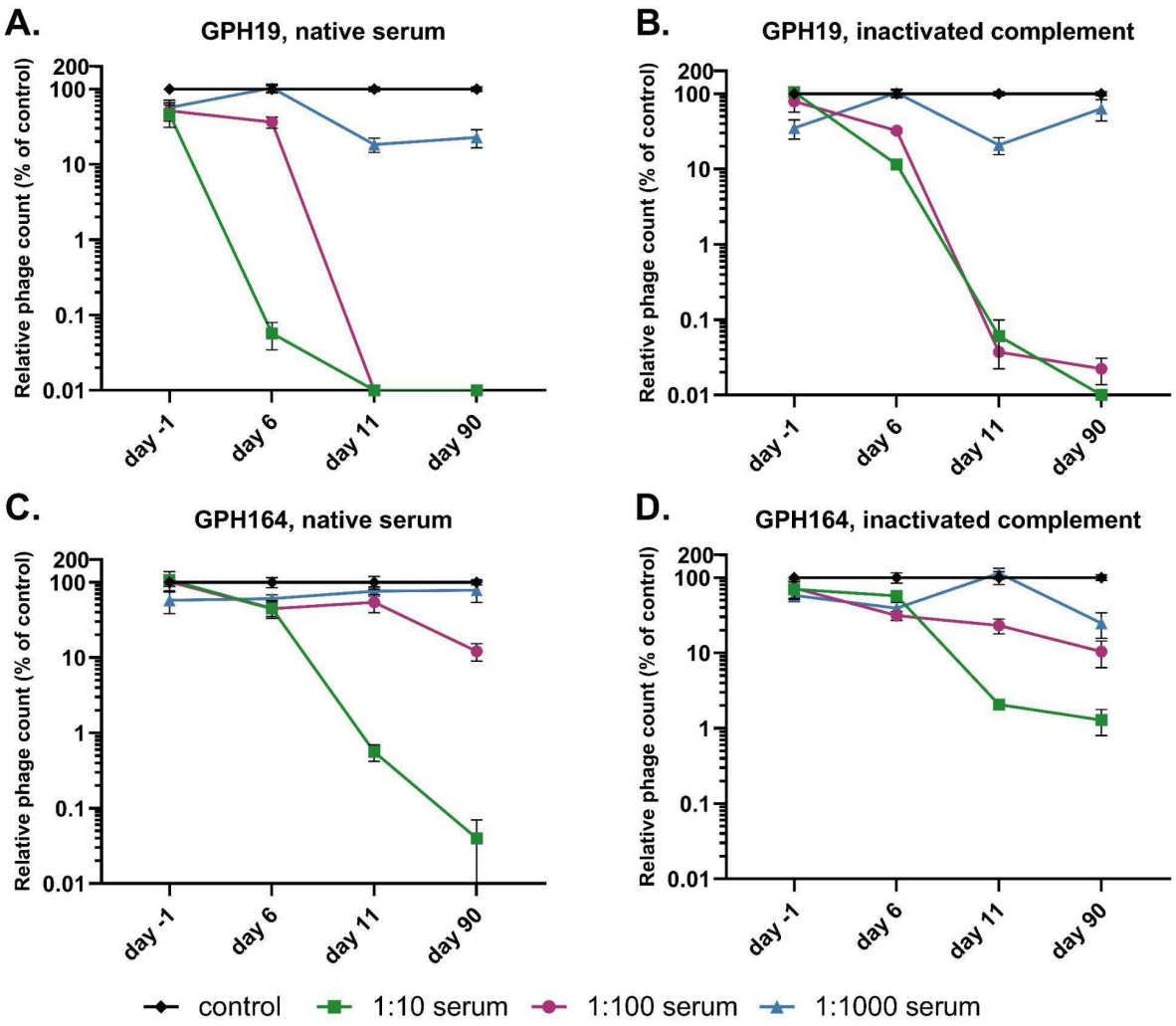


Figure 6. Serum-mediated neutralization of phages GPH19 and GPH164 before, during, and after phage therapy. Relative phage titres of GPH19 and GPH164 are expressed as percentages of the corresponding control condition following incubation with patient serum at dilutions of 1:10, 1:100, and 1:1000. Data are presented as mean ± SEM. A. neutralization of GPH19 with patient serum; B. neutralization of GPH19 with heat-inactivated serum of the patient; C. neutralization of GPH164 with patient serum; D. neutralization of GPH164 with heat-inactivated serum of the patient.

Plasma cytokine profiles during and after phage therapy

Systemic immune dynamics during treatment were assessed by longitudinal cytokine profiling. Four days before treatment, the patient developed a central venous catheter–related infection, which coincided with a marked increase in nearly all measured cytokines. A second cytokine peak occurred on day 14, three days after the final phage dose, and may have been associated with the post-treatment removal of the intramedullary catheter.

Across treatment and follow-up, the measured cytokines exhibited selective changes within five functional immune clusters (Figure 7). Within the infection-associated innate inflammation cluster, IL-6, TNF-α, and IL-18 showed modest overall declines, whereas IL-1β was undetectable throughout therapy. IL-6 additionally exhibited a small transient increase during days 1–3 of therapy before resuming its downward trajectory (Figure 7A). Within the interferon-associated pro-inflammatory axis, IFN-γ declined, whereas IFN-α2, CXCL9, and CXCL10 showed only minor fluctuations without a consistent overall trend (Figure 7B). The monocyte–macrophage recruitment and differentiation cluster showed a decrease in M-CSF, whereas MCP-1/CCL2 remained broadly stable (Figure 7C). The neutrophil mobilization and barrier immunity cluster showed a modest downward tendency, driven primarily by G-CSF. Similar to IL-6, G-CSF exhibited a transient increase during the first three days of treatment, whereas IL-8 remained broadly stable. IL-17A and IL-22 were below the assay's limit of detection throughout therapy (Figure 7D).

Among mediators associated with inflammatory resolution and type 2 reparative regulation, IL-10 increased modestly during therapy and declined during follow-up, whereas IL-1RA remained broadly stable despite minor fluctuations. IL-4 declined overall, although a small transient increase was observed during days 1–3 of therapy (Figure 7E). Collectively, the most apparent longitudinal changes involved modest reductions in innate inflammatory, IFN-γ-associated, granulopoietic, and macrophage differentiation signals, accompanied by a modest increase in IL-10 but no coordinated increase across reparative mediators.

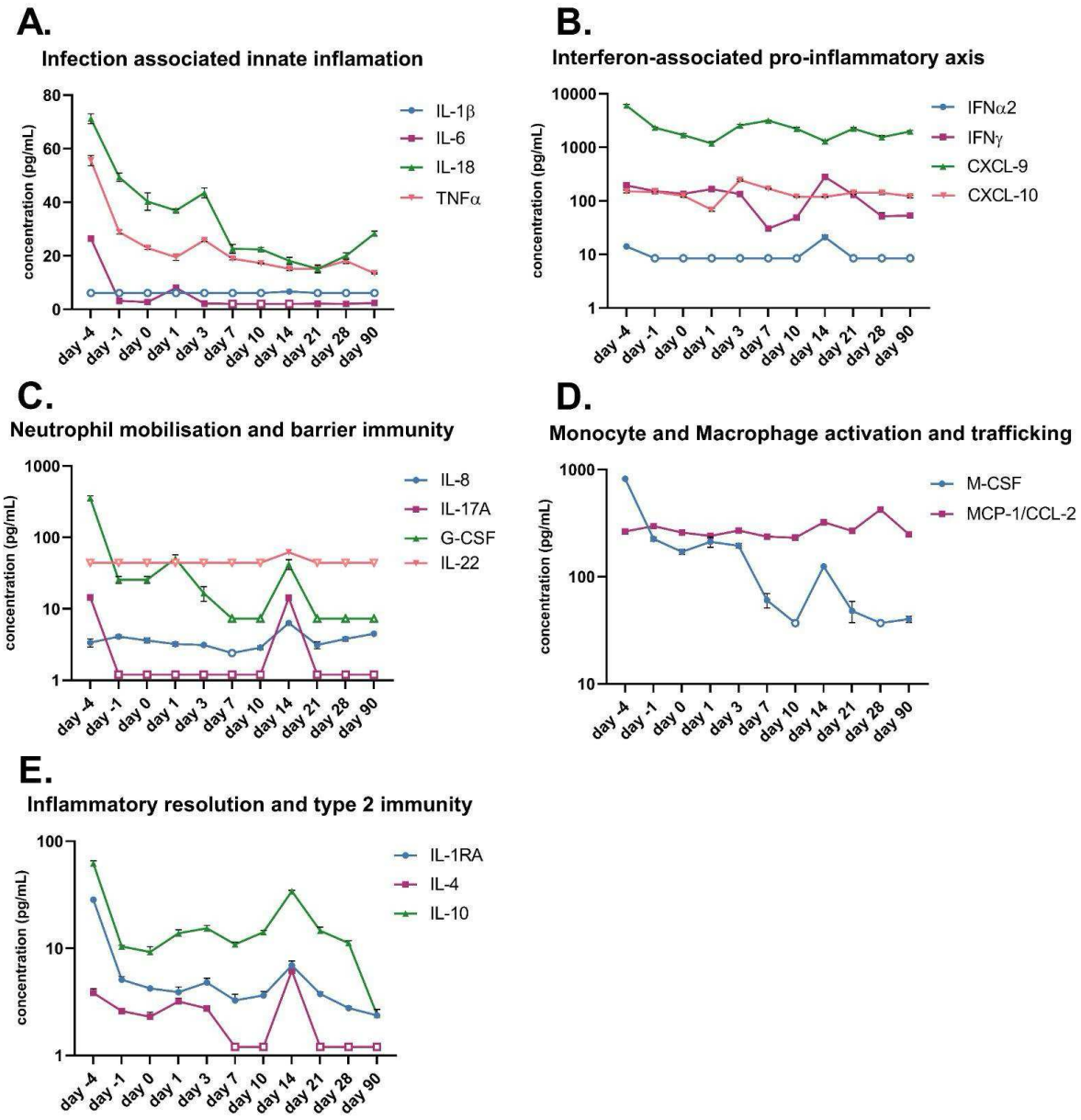


Figure 7. Plasma cytokine concentrations before, during, and after phage therapy. Cytokines were measured in plasma collected before treatment (days −4 and −1), during phage therapy (days 0-10), and during follow-up (days 14-90). Values below the lower limit of detection (LLOD) are plotted at the assay-specific LLOD and shown as open symbols. (A) Infection-associated innate inflammation: IL-1β, IL-6, TNF-α, IL-18, (B) Interferon–associated pro-inflammatory axis: IFN-γ, IFN-α2, CXCL9, CXCL10; (C) Neutrophil mobilization and barrier immunity: IL-8, IL-17A, G-CSF, IL-22; (D) Monocyte–macrophage recruitment and differentiation: MCP-1/CCL2, M-CSF; (E) Inflammatory resolution and type 2 reparative regulation: IL-10, IL-1RA, IL-4.

Discussion

The case demonstrates that the DPC therapy combined with targeted antimicrobial treatment and surgical interventions achieved a successful outcome of *K. pneumoniae* osteomyelitis in a war-related fracture. The multimodal delivery of bacteriophages (systemic, local, and through DAC hydrogel) was well tolerated. The systemic antibody response against the phages developed during the treatment, however, it was not directly associated with the treatment outcome. Management of chronic osteomyelitis caused by MDR *K. pneumoniae* remains a major clinical challenge, frequently requiring repeated surgical interventions, prolonged hospitalizations, and, in severe cases, amputation. In contemporary phage therapy practice, phages are typically administered locally at the site of infection and/or systemically, frequently in combination with antibiotics[40–45].

Russia's full-scale invasion of Ukraine has produced an increasing number of difficult-to-treat wound infections caused by Gram-negative bacteria, particularly *K. pneumoniae*. Published work on phage therapy for *K. pneumoniae* bone infections is confined to a number of clinical reports[41,42,45,46,47], among these several cases present a successful phage therapy of trauma-related infections[36,42,46,47]. Most of these reports describe a single route of phage administration - either systemic (i.v.) or local. In the presented case, a dual-phage therapy combined with antibiotics was administered both locally and systematically. Although the 2-year follow-up required to confirm infection eradication is ongoing, at 15 months after phage therapy (October 2026), the patient remained free of clinical symptoms, with marked improvements in limb function and diagnostic findings. These improvements were accompanied by decreased inflammatory markers (ESR and CRP), and normalization of plasma cytokine levels during the therapy, including reductions in markers of inflammation and immune activation (Figure 7). This is consistent with previous reports of phage therapy for complex osteoarticular infections[41,48] and peritonitis[49].

Beyond the favourable clinical outcome, this case demonstrates the clinical translation of a DPC strategy previously developed against the high-risk ST258 and ST512-KL107 lineage of *K. pneumoniae*. The sustained in vitro activity observed against the patient-derived isolate suggests that phage combinations designed to target heterogeneous bacterial populations may represent a promising translation approach for difficult-to-treat *K. pneumoniae* infections[38]. The clinical isolate also exhibited biofilm-forming capacity in vitro, a phenotype consistent with the chronic and persistent nature of osteomyelitis and providing additional biological rationale for the use of phages in this setting, although the anti-biofilm activity of the administered phages was not directly evaluated in this study.

In this case, local and systemic administration of GPH19 and GPH164 was followed by phage-specific antibody responses and serum neutralization. IgM increased during the first week, whereas IgG rose more gradually and reached its highest levels during late follow-up. These kinetics resembled a primary humoral response to novel phage antigens[22,28,50] despite detectable pretreatment reactivity against both phages, particularly GPH164 (Figure 4). Serum neutralizing activity was minimal before treatment but increased during therapy and follow-up, consistent with the development of a functional phage-specific immune response (Figure 6). GPH19 neutralization emerged by day 6 and was nearly complete at 1:10 and 1:100 dilutions by day 11, whereas GPH164 neutralization increased gradually through day 90 (Figure 6). Active phages were however recovered from blood only on day 1 and 2, whereas substantial neutralization was documented at later sampled time points. This apparent temporal mismatch may reflect fundamental differences between in vivo phage kinetics and the serum-only neutralization assay. Circulating phage titres may be influenced by cellular uptake and tissue distribution, which are not captured ex vivo, whereas replication on susceptible bacteria may have transiently supported phage recovery[51]. Importantly, the development of serum neutralizing activity did not preclude infection resolution or limb salvage.

The extensive antigen exposure associated with intraoperative local administration, continuous intramedullary delivery, and intravenous infusion may have contributed to the magnitude of the response. However, neutralizing activity can also develop after local administration alone. Eskenazi et al. reported substantial serum neutralization developed between days 8 and 18 in a patient receiving local phage therapy for a *Klebsiella*-infected wound associated with a femoral fracture. In both that patient and ours, neutralization developed without preventing a favourable clinical outcome[42]. These observations are compatible with a clinically useful interval during which phages may contribute to infection control before neutralization becomes substantial. However, individual cases cannot define the duration or clinical significance of such a therapeutic window.

A notable finding was the discordance between antibody binding and functional neutralization. Pretreatment serum predominantly recognized GPH164 in ELISA yet showed no detectable baseline neutralization. Moreover, GPH164 elicited broader and generally stronger ELISA reactivity, whereas GPH19 was neutralized more rapidly and efficiently (Figures 3, 4, and 5). Thus, total antibody binding did not predict the loss of phage infectivity. This distinction is biologically plausible because phage particles display multiple antigens, and antibodies targeting different proteins or epitopes may vary substantially in their neutralizing capacity[22,51]. ELISA confirms binding to phage antigens but does not establish whether the targeted epitopes are functionally relevant. Neutralizing activity is likely to depend on epitope location and accessibility, as well as the functional role of the bound phage protein.

Pre-treatment reactivity may have resulted from prior exposure to related phages in the human phageome or from cross-reactivity with non-phage antigens. Such antibodies may recognize phage epitopes without efficiently neutralizing the therapeutic phages. Pre-existing cross-reactive B-cell memory may also have shaped the subsequent response to GPH164 through antigenic imprinting, whereby preferential recall of previously primed clones could limit the recruitment of naïve B cells targeting novel, potentially neutralizing epitopes. The pronounced GPH164-specific IgA reactivity may likewise be consistent with prior mucosal exposure to a related antigen. Because IgA primarily mediates mucosal immunity, its contribution to systemic serum neutralization may be limited. At the same time, the IgM-first, IgG-later kinetics observed during therapy support the interpretation that pretreatment reactivity did not represent a fully developed response to the administered phages. Further studies are required to elucidate these mechanisms.

Heat inactivation attenuated serum neutralization under selected conditions, most clearly at a 1:10 dilution for GPH19 on day 6 and GPH164 on days 11 and 90, although this effect was not uniform across conditions (Figure 6). Because substantial neutralizing activity was retained after heat treatment, complement likely acted in concert with phage-specific antibodies rather than as the sole effector. Antibodies may engage complement through the classical pathway, activating a cascade that promotes phage inactivation, although the precise mechanisms involved remain incompletely understood. These results extend previous experimental evidence that serum factors, including complement, can influence phage inactivation, pharmacokinetics, and bioavailability[22,40–44,50], and, to our knowledge, provide the first clinical observation suggesting a contribution of complement to serum neutralization during phage therapy[52].

This study has several limitations. First, it describes a single patient, and the findings cannot be generalized to broader populations. Second, phage therapy was combined with antibiotics and multiple surgical procedures, preventing attribution of the favourable outcome to any individual intervention. Third, heat inactivation alone cannot fully establish a complement-dependent mechanism. Fourth, the healthy reference cohort may not reflect the patient's demographic characteristics or history of environmental phage exposure. Finally, although no clinical recurrence was observed during 15 months of follow-up, longer observation is required to confirm recurrent infection eradication.

Despite these limitations, this study demonstrates the successful treatment of a difficult, refractory *K. pneumoniae* infection using specific, individually selected bacteriophages in combination with antibiotics. Favourable clinical outcomes and limb salvage were achieved despite the simultaneous development of an effective immune response against the administered phages. This case provides encouraging evidence for future therapeutic approaches involving bacteriophages and highlights the potential of phage therapy as a

rescue treatment. We believe that these findings support the further development and broader implementation of phage therapy.

In conclusion, our work shows a successful case of multimodal phage treatment with phages GPH19 and GPH164, that was associated with sustained infection control and limb salvage in refractory MDR *K. pneumoniae* osteomyelitis. The pre-established DPC, selected for complementary activity against distinct bacterial subpopulations, retained activity against the patient-derived isolate, supporting its potential translation to difficult-to-treat infections caused by high-risk *K. pneumoniae* lineages. Despite detectable pre-treatment reactivity, both phages elicited a humoral response similar to primary immune response, with IgM first and IgG later. The presence of neutralizing antibodies did not prevent infection control or limb salvage.

METHODS

Patient and ethical approval

This report describes a single patient treated at Riga East Clinical University Hospital in Riga, Latvia. The study was approved by the Central Medical Ethics Committee (Nr. 01-29.1.2/5916). Written informed consent was obtained from the patient for both the treatment and the publication of this case report. Patient identity has been anonymized throughout. This case report was prepared in accordance with the CARE (CAse REport) guidelines.

Phage preparation and quality control

A pre-established anti ST512-KL107 DPC, including two lytic phages, GPH19 and GPH164, originating from the GENeva PHage Collection (GENPH), were selected for patient treatment. Phage preparations were produced and quality-controlled at the JAFRAL laboratory (Slovenia), in accordance with quality and safety standards for small-scale phage production for human application. Quality control of the final phage stocks included confirmation of phage identity and titre, assessment of pH, and measurement of endotoxin levels, ensuring suitability for clinical use. For patient phages were prepared at JAFRAL GMP facility at the titre of 5×10^9 PFU/mL, endotoxin level 0,5 EU/mL; total aerobic microbial count (TAMC) 0 CFU/mL; total yeast and mold count (TYMC) 0 CFU/mL; pH 7.03; colourless, clear liquid without any visible particles. The DPC was diluted to 10^7 PFU/mL for treatment, delivered intravenously as a 70mL infusion over 7h (1 mL/kg) and corresponding to a total delivered dose of 7×10^8 PFU per phage per day. The same two phages, each at 1×10^7 PFU/mL, were administered intramedullary by continuous infusion of 2.5mL/h over 20h, giving a total volume of 50mL and local dose of 5×10^8 PFU per phage per day.

Phage susceptibility testing

Three to four *K. pneumoniae* colonies from an agar plate were inoculated into 5 mL of tryptic soy broth (TSB) and incubated at 35 °C with shaking at 150 rpm for 2.5 h, corresponding to a density of approximately 0.5 McFarland. 100µL of the bacterial suspension was mixed with 4-5 mL of molten 0.7% tryptic soy agar (TSA) and poured onto TSA Petri plates. After 15-20 min of solidification, 10 µL of phage suspension was spotted onto the agar surface. Plates were maintained at room temperature for approximately 30 min to allow the drop to dry, then incubated inverted at 35 °C for 18h. Lysis patterns were recorded as follows: ++++, confluent lysis; +++, semiconfluent lysis; ++, partial lysis; or no lysis.

Determination of efficiency of plating

To assess phage activity against RSU-KP-Osteomyelitis1, EOP was determined by comparing phage titres obtained on the original host (with known susceptibility) with those obtained on the patient isolate. Serial tenfold dilutions of phages (10^{-1} to 10^{-9} in sterile 0.9% NaCl) were prepared. Bacterial suspensions were obtained by inoculating 3-4 colonies from agar plate into 5 mL of TSB and incubating at 35 °C with shaking at 150 rpm for 2.5 h. A 100 µL aliquot of bacterial suspension was mixed with 50 µL of phage dilution and 5 mL of molten 0.7% TSA, poured onto plates, dried for 15-20 min, and incubated inverted at 35 °C for 18 h. All assays were performed in triplicate.

Preparation of antimicrobial dilutions and determination of MIC

Stock solutions of antimicrobials were prepared by dissolving antibiotics in sterile Mueller–Hinton (MH) broth at the following concentrations: gentamicin, 64 mg/L; ceftazidime/avibactam, 64 mg/L; colistin, 64 mg/L; and tigecycline, 16 mg/L. MIC testing was performed using serial twofold dilutions in 96-well microplates (Nunclon Delta Surface, Thermo Scientific, Denmark) in accordance with EUCAST guidelines. Plates were incubated at 35 °C for 18 h, and bacterial growth was measured by optical density at 600 nm (OD600) using a Thermo Scientific Varioskan Lux Multimode Microplate Reader (Thermo Fisher Scientific, USA). The MIC was defined as the lowest antimicrobial concentration at which bacterial growth was inhibited (OD < 0.1).

MOI of phages

The MOI was defined as the ratio of PFU to host bacterial cells (CFU). Phage concentrations were determined by plaque assay, and bacterial counts were determined by CFU enumeration. Infection assays were performed at MOI values of 0.1, 1, and 10 by mixing appropriate volumes of phage suspensions with bacterial cultures.

Assessment of biofilm formation by crystal violet assay

The bacterial concentration of the patient-derived *K. pneumoniae* isolate was standardized by colony-forming units (CFU) enumeration, with a 0.5 McFarland suspension corresponding

to 7.8 × 10^7 CFU/mL. Biofilm formation was quantified using the crystal violet staining method, following Stepanović et al.[53]. Patient *K. pneumoniae* colonies (3–5) were grown in Luria–Bertani (LB) broth for 24h at 35 °C, and suspensions were adjusted to 1:100 dilutions in LB. Serial dilutions in sterile 0.9% NaCl were prepared for CFU enumeration to ensure 25–250 colonies per plate. Aliquots of 200 µL of bacterial suspension were dispensed into 96-well plates (TC plate; Suspension, F, Sarstedt, Germany) (27 wells per isolate). Controls included sterile LB (negative control) and *Klebsiella quasipneumoniae* ATCC 700603 (positive control). Plates were incubated at 35°C for 6, 12, 24, 36, and 48 h, sealed with parafilm. Following incubation, planktonic cells were removed and wells were washed twice with 250 µL saline. Biofilms were stained with 0.1% crystal violet for 20 min, washed three times with distilled water, and de-stained with 200 µL of 96% ethanol. Optical density at 600 nm (OD600) was measured using a Thermo Scientific Varioskan Lux Multimode Microplate Reader (Thermo Fisher Scientific, USA).

Determination of phage concentration in patient serum

Phage titres in serum were determined using the plaque assay. Serum was obtained from 4-5 mL of blood collected 2 h after intravenous phage administration. Serum samples were collected into BD Vacutainer® serum tubes (BD, USA), serum was separated by centrifugation (15 min, 3400 x g, room temperature), then stored at -80°C for further use.

A 100 µL aliquot of bacterial suspension was mixed with 50 µL of serum sample, and the assay was performed as described for the plaque assay method above. Each experiment was performed in triplicate.

Phage preparation for ELISA

GPH19 and GPH164 phages and host bacterial strains were obtained from JAFRAL. All phage lysates were prepared in enriched nutrient broth inoculated with an appropriate overnight bacterial host suspension. Phage host strains were grown at 35°C to OD600=0.4 and then phage was added at a final titre of 10^6 PFU/mL. The culture was then incubated at 37°C with vigorous shaking for 6 h and transferred to 4 °C for 2 days for clarification.

All phage lysates were centrifuged at 10,000 x g, 4°C for 10 min, and the supernatants were filtered through 0.45 µm and 0.22 µm Millipore PES membrane filters (Merck Millipore).

Phage purification for ELISA

Tangential flow filtration (TFF, Hollow Fiber) was used as an initial clarification and buffer exchange step to concentrate the sample and remove low-molecular-weight impurities. The starting material (1L) was concentrated using a Spectrum hollow fibre cartridge (115 cm^3) with a nominal MWCO of 750 kDa. The sample was reduced to a final volume of 50 mL under controlled flow conditions. Buffer exchange was then performed by diafiltration using 5

diafiltration volumes (DV) with 50 mM Tris, 50 mM NaCl, pH 7.4. Following diafiltration, the retentate was sequentially filtered through 0.45 µm and 0.22 µm syringe filters.

Capto™ Core 700 chromatography was employed as a flow-through polishing step to remove low-molecular-weight contaminants, including host cell proteins, nucleic acids, and soluble endotoxins. A HiScreen Capto™ Core 700 (Cytiva) column (bed volume: 4.7 mL) was equilibrated with 5 column volumes (CV) of 50 mM Tris, 50 mM NaCl, pH 7.4, at a flow rate of 2 mL/min. The sample was loaded at the same flow rate (2 mL/min), and phages were collected in the flow-through fraction. The column was washed with 5 CV of water, followed by 1 M NaOH containing 30% isopropanol (minimum contact time: 60 min), and subsequently rinsed with 5–10 CV of water. The column was stored in 20% ethanol or re-equilibrated in a buffer prior to reuse.

Anion exchange chromatography using Capto™ Q was employed to separate negatively charged components based on their surface charge properties and to remove endotoxin-associated contaminants, including outer membrane vesicles. A HiScreen Capto™ Q column (4.7 mL) was equilibrated with 5 CV of: 50 mM Tris, 50 mM NaCl, pH 7.4, flow rate: 2 mL/min. Then the sample from the previous step (flow-through from Capto Core) was loaded at 0.5 mL/min to enhance binding efficiency. The column was washed using an equilibration buffer at 2 mL/min. Bound components were eluted using a stepwise NaCl gradient: 100 mM NaCl, 200 mM NaCl and final strip with 2 M NaCl was performed. Each wash step was performed at 2 mL/min. Fractions were collected manually into 96-well plates. A buffer blank was included as a reference. Absorbance at 280 nm (A280) was measured using a microplate reader. Elution peaks were identified based on absorbance profiles, and selected fractions were pooled and 0.22µm filtered for further analysis (Titre, Endozyme and TEM microscopy).

ELISA

Each well of a 96-well plate was coated separately with 100 µL of purified phage (titre 1×10^9 PFU/ml). To measure background absorbance, some wells were coated with a PBS buffer. The plates were incubated overnight at 4°C. The next day, the wells were emptied and washed five times with 100 µL PBS. Then, 150 µL of SuperBlock (Thermo Fisher) diluted 1:5 in PBS was added to block uncoated areas of the wells. Plates were incubated 45 minutes at room temperature, after which the wells were emptied and washed five times with 100 µL PBS + 0.05% Tween 20. Investigated sera diluted 1:100 in PBS was added to the wells, and the plate was incubated 2 hours at 37°C. The wells were then emptied and washed five times with PBS + 0.05% Tween 20. Next, 100 µL of HRP-conjugated anti-human antibodies diluted in PBS (IgM 1:200,000; IgG 1:100,000; IgA 1:100,000) were added to each well. The plate was incubated 1 hour at room temperature in the dark, then emptied and washed five times with PBS + 0.05% Tween 20. Finally, 50 µL of TMB was added to each well and incubated for 25 minutes at room temperature in the dark. The reaction was stopped with 25 µL of 2 N H_2SO_4.

Absorbance was measured at 450 nm and 550 nm, and the result was calculated as A_{450} – A_{550}.

Healthy volunteers' sera were pre-tested and based on ELISA OD. Highly responsive sera were selected as the reference to calculate ELISA units (EU) comparable between plates and independent readings. Briefly, to calculate EU, 10 points of standard serum dilutions were determined on each plate. The dilution giving an optical density at 450 nm (OD450) of 1 was assigned as 1,000 EU and then 500 EU, 250 EU, 125 EU, etc. The obtained standard curve was fitted to a function that converted OD values to EU. Each EU was normalized, and the average value of each duplicate was calculated. These values were presented in groups and statistically analyzed.

Reference sera of healthy volunteers

Serum samples from healthy volunteers who had never been subjected to phage therapy or involved in phage work (n 50) were collected into standard clotting tubes (BD SST II Advance), left for 1 hour at room temperature (RT) to clot and serum was separated from the clot by centrifugation (15 min, 2000 x g, RT), then stored at -20°C for further use. The written informed consent form had been reviewed and approved by the local Commission of Bioethics in Wrocław and collected from each patient prior to blood collection (approval number: KB/02/2020). Sera demonstrating high OD by ELISA were selected as the reference sera.

Determination of serum neutralization capacity

Patient serum samples were evaluated for phage-neutralizing activity under two conditions: (1) serum with active complement, and (2) heat-inactivated serum (56 °C for 30 min) to eliminate complement activity. 50µL of 10^6 Phages were incubated with 450µL diluted serum samples at 37 °C for 1 h, and residual infectious phages were quantified by plaque assay on either of the host strains. Efficiency of plating (PFU/mL) was compared between test and control samples (phages without serum) to determine the neutralization effect.

Determination of cytokine concentrations

Plasma samples were collected into EDTA tubes; plasma was separated by centrifugation (15 min, 3400 g, room temperature), then stored at -80°C for further use.

The concentrations of 18 chemokines and cytokines were measured using the Luminex® 200™ System (Diasorin) and MILLIPLEX® Human Cytokine/Chemokine/Growth Factor Panel A (Merck KGaA). Results were analyzed using Belysa 1.2.2 software. Concentrations of analytes below the detection limit were replaced with the minimum detectable value, according to the manufacturer's protocol. Detection sensitivities (pg/mL) were as follows: G-CSF, 7.30; IFNα2, 8.50; IFNγ, 2.40; IL-1β, 6.10; IL-1RA, 1.20; IL-4, 1.20; IL-6, 2.00; IL-8, 2.40; IL-

17A, 1.20; IL-18, 0.98; IL-22, 44.00; IP-10, 2.90; MCP-1, 3.70; M-CSF, 37.00; CXCL9, 24.00; and TNFα, 4.90.

PET/CT imaging

Whole-body ^{18}F-FDG PET/CT scans were performed from the top of the head, including the extremities. Additionally, low-dose CT was performed to process attenuation correction (CT-AC) and used for anatomical co-registration of PET findings. ^{18}F-FDG PET/CT images were acquired 60–75 min after the intravenous injection of ^{18}F-FDG (3.3 MBq per kg), using an ^{18}F-FDG PET/CT combined with a third-generation multi-slice spiral CT scanner with a dedicated full-ring PET scanner, which had a high-count-rate-capability lutetium-yttrium oxyorthosilicate (LYSO)-based camera with time-of-flight (TOF) technology. Emission scans of ^{18}F-FDG PET/CT were acquired 45 s–2 min per bed in 3D mode. PET and CT images (non-corrected and attenuation-corrected) were evaluated in a rotating maximum-intensity projection and a cross-sectional plane view (transverse–sagittal–coronal). Images with increased focal uptake, with higher intensity than surrounding tissues, which did not correspond to the physiological distribution of ^{18}FDG, were defined as positive.^{18}FDG, were defined as positive.

Bacterial isolate whole genome sequencing

Prior to whole genome sequencing, the total DNA was extracted from several suspended individual colonies picked from a Petri dish after overnight incubation in the case of both strains of interest. For preparation of the DNA, proteinase K/SDS treatment followed by DNA concentration and purification according to the Genomic DNA Clean & Concentrator-10 Kit (Zymo Research) protocol was performed.

In case of short-read sequencing, the isolate from surgical material, the extracted DNA (~1000 ng) was then used as input to prepare Illumina MiSeq-compatible DNA libraries for 250 bp paired-end read sequencing using the QIAseq FX DNA Library Kit as per the manufacturer's instructions (using adapter #24 from QIAseq UDI Y-Adapter Kit 24 for this particular library) up to the PCR step (No PCR was employed in this case). The resultant library was sequenced on the Illumina MiSeq system as one of the several individually barcoded pooled libraries using the 500-cycle MiSeq Reagent Kit v2. Demultiplexing of the pooled sequencing data was carried out based on the adapter sequences used, and demultiplexed reads were trimmed using fastp52 (v0.20.0.; employing default parameters with detection of any remaining adapter sequences enabled).

For long-read sequencing, library preparation was then generally carried out in accordance with the ONT Rapid Barcoding Kit 24 V14 (SQK-RBK114.24) Nanopore-only Microbial Isolate Sequencing Solution (NO-MISS) protocol, using an individual barcode prior to pooling with other barcoded samples. The resulting library was sequenced using the FLO-MIN114 flow

cell (R10.4.1) on a MinION Mk1D device. Basecalling was performed using the dna_r10.4.1_e8.2_400bps_sup@v5.0.0 model and was followed by demultiplexing. Demultiplexed reads from three distinctly barcoded samples (Barcodes #10, #22, and #24, with the first one and the two other representing different DNA extractions that were parts of different runs sequenced using different chips) were concatenated and filtered using Filtlong (v0.2.1; --keep_percent 90 --min_length 1000).

Both short and long trimmed read datasets were de novo assembled using Hybracter[54] (v0.12.0.) in hybrid mode with default settings.

Trimmed read datasets metrics were summarized using SeqKit56 (v2.5.1.). The resulting de novo assembly was evaluated with CheckM2[55] (v1.1.0) and annotated for Klebsiella-associated features of interest with the help of Kleborate17 (v3.3.0b1), Klebsiella pneumoniae species complex preset - "kpsc"), before upload to GenBank requesting annotation using the latest version of PGAP[56].

DPC of GPH19/GPH164

A previously defined DPC targeting capsule type KL107 associated with ST512 was used for phage treatment. To identify candidate phages, we used a *K. pneumoniae* host strain, a clinical ST512 strain from a previous patient that was eligible for phage therapy. As phage resistant subpopulations frequently emerge in *K. pneumoniae*, generally by capsule loss mechanisms, the non-encapsulated *K. pneumoniae* sub-population[57] was isolated using a Percoll density gradient. Briefly, 20 mL of bacterial culture were incubated at 37°C with shaking for approximately 4 h, until OD_{600nm} exceeded 1.0. The cultures were then centrifuged at 7,800 x g for 10 min, and the pellet was resuspended in 1 mL of PBS. In a 1.5 mL Eppendorf tube, 650 µL of the concentrated bacterial suspension were mixed with 650 µL of Percoll, gently inverted, and centrifuged at 14 000 x g for 10 min at 4°C. From this gradient, two bacterial fractions were resolved: a light (L) fraction corresponding to capsulated bacteria and the heavy (H) fraction corresponding to non-capsulated bacteria[58].
Bacterial lawns from the clinical strain and its H fraction were prepared on LB soft agar, and 5 µL of each phage from the entire GENPH Collection, comprising approximately 150 anti-*K. pneumoniae* characterized phages isolated from wastewaters[59], were spotted onto the surface. GENPH phages showing lytic activity were then propagated on either host strain and titrated against both the WT strain and the heavy variant. Phages yielding titres of $\geq 10^8$ PFU/mL were retained for further analysis. A phage displaying clear lytic plaque on encapsulated bacteria was selected and combined with a phage displaying clear lytic plaque on non-encapsulated bacteria.
Liquid infection assays were then performed. The density of host strain culture was adjusted in 0.9% NaCl to 0.5 McFarland and then diluted 1:100 in cation-adjusted Mueller Hinton broth

to obtain a final concentration of 1.5 x 10^6 CFU/mL. Aliquots of 990 µL were dispensed into each well of the plate, followed by the addition of 10 µL of the corresponding bacteriophage preparation to achieve final MOIs of 1 and 0.1. The plate was incubated for 18 h in a plate reader, with optical density measurements recorded every 30 min. Wells containing bacteria alone were included as controls for bacterial growth. All experiments were performed in biological triplicates. The DPC selected based on complementary activity against encapsulated and non-encapsulated derivatives.

Phage whole-genome sequencing

GPH19 and GPH164 were propagated separately to a titre of 10^9 PFU/mL. For each phage, 2 mL of lysate was centrifuged at 20,000 × g for 20 min at 4 °C. The supernatant was discarded, and the pellet was resuspended in nuclease buffer containing DNase (0.02 mg/mL) and RNase (0.1 mg/mL), followed by incubation at 37 °C for 1 h. EDTA was then added to a final concentration of 20 mM, and the samples were centrifuged again at 20,000 × g for 20 min at 4 °C. The supernatant was discarded, and DNA was extracted from the pellet using the Wizard HMW DNA Extraction Kit (Promega, A2920), according to the manufacturer's instructions.

Extracted DNA was quantified using a Qubit fluorometer (Thermo Fisher Scientific). Sequencing libraries were prepared using 100 ng and SQK-RPB114.24 kit, according to the manufacturer's instructions. Libraries were loaded onto R10.4.1 flow cells (FLO-MIN114) and sequenced on a GridION instrument (Oxford Nanopore Technologies). Live basecalling was performed in super-accuracy mode using the dna_r10.4.1_e8.2_400bps_sup@v5.2.0 model.

Statistical analysis

All statistical analyses and data visualization were performed using GraphPad Prism software 10.6.1. (GraphPad Software, San Diego, CA, USA). Data are presented as mean ± standard deviation (SD) unless otherwise stated. The results were analyzed using the ANOVA test. A p value of < 0.05 was considered statistically significant.

Data availability

The supplementary data generated in this study are provided in the Supplementary Information. The data presented in this study are available on request from the corresponding author. The data is not publicly available due to patient privacy.

The complete genome sequences of phages have been deposited in the National Center for Biotechnology Information (NCBI) GenBank under SRA accession numbers: SRR41552962 and SRR41552963.

The complete genome sequences of bacteria have been deposited in the National Center for Biotechnology Information (NCBI) GenBank JCFYWV000000000 and under Biosample accession number SAMN64511890. Accession numbers for the genome sequences are SRR41443480 and SRR41443481.

Conflicts of interest

The authors declare no conflict of interest.

Funding statement

The research received funding from the project: "*New knowledge and approaches to reduce antimicrobial resistance, limit the spread of HIV and expand community vaccination coverage*" (VPP-VM-Sabiedrības_Veselība-2023/5-0001).

The research was funded by Rīga Stradiņš University (RSU), Faculty of Medicine, through the pilot project *"Professor J.Kroiča's Scientific Unit".*

The GENeva PHage (GENPH) Collection was funded by the Fondation Privée des HUG (Geneva University Hospitals, STARTER Grant No. RS07-03 to DOA), Research and Development Program scheme PRD 9-2020-II (DOA), and Fondation Ernst et Lucie Schmidheiny (RS).

KD acknowledges support from the National Science Centre in Poland: grant no. 2019/35/B/NZ7/01824.

Acknowledgements

We are most grateful to Frenk Smrekar from Jafral for producing and providing phages used for this study and Zita Kustova for daily care for patient and sample collection.

The authors used Claude (https://claude.ai) to help write earlier versions of text and edit it after which the content was reviewed and edited by the authors, and to provide suggestions for colour scheme and layout for Figure 1.

Conceptualization, J.K., K.R., K.D., L.B., R.R.A., R.S.; Methodology, A.W., D.E., D.O.A., D.R., I.R., K.D., K.R., K.S., L.B., L.F., L.S., M.M., M.R., N.B., N.Z., R.R.A., R.S., S.M., Z.M.K.; Software, L.B., R.R.A.; formal analysis, D.E., D.O.A., K.D., K.R., L.B., M.R., R.R.A., R.S., S.M., Z.M.K.; Investigation, D.E., D.O.A., K.R., L.B., M.R., N.Z., R.R.A., R.S., S.M.; Investigation-Surgery, D.E., D.R., K.P., K.R., J.M., M.K., M.M.; Data Curation, D.O.A., K.D., K.R., L.B., M.R., N.Z., R.R.A., R.S., Z.M.K.; Writing-Original draft preparation, D.O.A., K.D., K.R., L.B., M.K., M.R., R.R.A., R.S., Z.M.K.; Writing-Review and editing, D.E., D.O.A., K.D., K.R., L.B., R.R.A., L.S., N.Z., R.S., Z.M.K.; Visualization, J.M., K.D., K.R., L.B., M.K., R.R.A., R.S., Z.M.K.; Supervision, J.K., K.D., K.R., R.S. All authors have read and agreed to the published version of the manuscript.

Author information:

These authors contributed equally: Renate Ruta Apse, Lise Berentsen

Renate Ruta Apse[1], Lise Berentsen[1], Sandis Maurins[1], Dace Eglite[1,6], Nikita Zrelovs[1,9], Krystyna Dabrowska[13,14,15], Zuzanna Maria Kazmierczak[13,15], Roberto Sierra[16,18], Diego O. Andrey[16,17,18], Léna Falconnet[16], Mélanie Roch[16], Nikola Brauca[1], Laima Sevastjanova[1], Kitija Straumane[1,6], Juta Kroica[1], Monta Madelane[2,3,7], Dace Rudzite[10], Jevgenijs Movcans[8], Konstantins Plotnikovs[8], Anda Vilmane[12], Marika Kalnina[11], Izabela Rybicka[15], Aleksandra Wilczak[13], Karlis Racenis[1,2,5]

[1]Department of Biology and Microbiology, Riga Stradins University, LV-1007 Riga, Latvia
[2]Department of Internal Diseases, Riga Stradins University, LV-1007 Riga, Latvia
[3]Department of Infectology, Riga Stradins University, LV-1007 Riga, Latvia
[4]Institute of Microbiology and Virology, Rīga Stradins University Research Center, LV-1067 Riga, Latvia
[5]Center of Nephrology, Pauls Stradins Clinical University Hospital, LV-1002 Riga, Latvia
[6]Joint Laboratory, Pauls Stradins Clinical University Hospital, LV-1002 Riga, Latvia
[7]Department of Infection Control, Riga East Clinical University Hospital, LV-1079 Riga, Latvia
[8]Department of Traumatology and Orthopedics, Riga East Clinical University Hospital, LV-1079 Riga, Latvia
[9]Latvian Biomedical Research and Study Centre, LV-1067 Riga, Latvia
[10]Joint Laboratory, Riga East Clinical University Hospital, LV-1079 Riga, Latvia
[11]Nuclear Medicine Clinic, ARS, LV-1010 Riga, Latvia
[12]Institute of Microbiology and Virology, Riga Stradins University Research Centre, LV-1067 Riga, Latvia
[13]Laboratory of Phage Molecular Biology, Hirszfeld Institute of Immunology and Experimental Therapy, Polish Academy of Sciences, 53-114 Wroclaw, Poland
[14]Research & Development Center, Regional Specialist Hospital, 51-124 Wroclaw, Poland
[15]Faculty of Medicine, Wroclaw University of Science and Technology, 50-370 Wroclaw, Poland
[16]Department of Microbiology and Molecular Medicine, Faculty of Medicine, University of Geneva, CH-1211 Geneva, Switzerland
[17]Division of Infectious Diseases, Department of Medicine, Geneva University Hospitals and Medical School, 1205 Geneva, Switzerland
[18]Department of Diagnostics, Geneva University Hospitals and University of Geneva, 1205 Geneva, Switzerland

ORCID numbers for authors:

1. Juta Kroiča: 0000-0003-0805-7063
2. Kārlis Rācenis: 0000-0001-7123-4048
3. Dace Eglīte: 0000-0001-5675-5320
4. Laima Sevastjanova: 0000-0001-6091-0004
5. Nikola Brauča: 0009-0009-2196-3133
6. Sandis Mauriņš: 0000-0002-4403-1728
7. Renāte R. Apse: 0000-0001-7119-8403

8. Lise Berentsen: 0009-0008-0822-4240
9. Kitija Straumane: 0009-0005-0451-4150
10. Ņikita Zrelovs: 0000-0001-7429-5962
11. Krystyna Dabrowska: 0000-0002-1518-3183
12. Zuzanna Maria Kazmierczak: 0000-0001-7220-3518
13. Izabela Rybicka: 0000-0003-2083-1592
14. Aleksandra Wilczak: 0000-0003-0085-4092
15. Monta Madelane: 0000-0003-2950-5435
16. Dace Rudzite: 0009-0008-3478-5703
17. Jevgenijs Movcans: 0000-0003-0561-4696
18. Diego Andrey: 0000-0003-3247-9274
19. Roberto Sierra: 0000-0002-8657-1781
20. Melanie Roch: 0000-0001-6485-8434
21. Léna Falconnet 0009-0002-3582-1282
22. Marika Kalnina: 0000-0002-0456-7368
23. Konstantins Plotnikovs: 0000-0002-6631-9343
24. Anda Vilmane: 0000-0002-1738-013X

References

1. Ghieh, F., Bizri, A. R., Beaineh, P., Chalhoub, R. & Abu Sittah, G. Systematic review of the microbiology of osteomyelitis associated with war injuries in the Middle East and North Africa. *Medicine, Conflict and Survival* **39**, 150–161 (2023).
2. Ljungquist, O. *et al.* Highly multidrug-resistant Gram-negative bacterial infections in war victims in Ukraine, 2022. *The Lancet Infectious Diseases* **23**, 784–786 (2023).
3. Kondratiuk, V. *et al.* Antibiotic resistance characteristics and genetic determinants of hypervirulence in Klebsiella pneumoniae isolated from wounded individuals in Ukraine. *Journal of Hospital Infection* **167**, 232–237 (2026).
4. Holubnycha, V. M. & Kholodylo, O. V. War impact on antimicrobial resistance and bacteriological profile of wound infections in Ukraine. *Commun Med* **5**, 394 (2025).
5. Ljungquist, O. *et al.* Pandrug-resistant Klebsiella pneumoniae isolated from Ukrainian war victims are hypervirulent. *Journal of Infection* **89**, 106312 (2024).
6. Schreiber, S. *et al.* War injuries and antimicrobial resistance: what impact do multi-resistant pathogens have on the treatment of Ukrainian war- wounded patients? *Eur J Trauma Emerg Surg* **52**, 60 (2026).

7. Costescu Strachinaru, D. I. *et al.* Management and Prevention of Multidrug-Resistant Bacteria in War Casualties. *TropicalMed* **10**, 128 (2025).
8. Sandfort, M. *et al.* Increase in NDM-1 and NDM-1/OXA-48-producing Klebsiella pneumoniae in Germany associated with the war in Ukraine, 2022. *Eurosurveillance* **27**, (2022).
9. Navon-Venezia, S., Kondratyeva, K. & Carattoli, A. Klebsiella pneumoniae: a major worldwide source and shuttle for antibiotic resistance. *FEMS Microbiology Reviews* **41**, 252–275 (2017).
10. Masters, E. A. *et al.* Evolving concepts in bone infection: redefining “biofilm”, “acute vs. chronic osteomyelitis”, “the immune proteome” and “local antibiotic therapy”. *Bone Res* **7**, 20 (2019).
11. Polyzou, E. *et al.* Managing Bone Infections Beyond Systemic Antibiotics: A Scoping Review. *Pathogens* **15**, 201 (2026).
12. Wang, Y. & Yu, Y. Phage therapy as a revitalized weapon for treating clinical diseases. *Microbiome Res Rep.* **4**, (2025).
13. Liu, S., Lu, H., Zhang, S., Shi, Y. & Chen, Q. Phages against Pathogenic Bacterial Biofilms and Biofilm-Based Infections: A Review. *Pharmaceutics* **14**, 427 (2022).
14. Kortright, K. E., Chan, B. K., Koff, J. L. & Turner, P. E. Phage Therapy: A Renewed Approach to Combat Antibiotic-Resistant Bacteria. *Cell Host & Microbe* **25**, 219–232 (2019).
15. Geneviève, J., McCallin, S., Huttner, A., Pham, T.-T. & Suva, D. A systematic review of phage therapy applied to bone and joint infections: an analysis of success rates, treatment modalities and safety. *EFORT Open Reviews* **6**, 1148–1156 (2021).
16. Suh, G. A., Ferry, T. & Abdel, M. P. Phage Therapy as a Novel Therapeutic for the Treatment of Bone and Joint Infections. *Clinical Infectious Diseases* **77**, S407–S415 (2023).
17. Lam, M. M. C. *et al.* A genomic surveillance framework and genotyping tool for Klebsiella pneumoniae and its related species complex. *Nat Commun* **12**, 4188 (2021).
18. Ørskov, I. & Ørskov, F. 4 Serotyping of Klebsiella. in *Methods in Microbiology* vol. 14 143–164 (Elsevier, 1984).

19. Lourenço, M. *et al.* Phages against Noncapsulated Klebsiella pneumoniae: Broader Host range, Slower Resistance. *Microbiol Spectr* **11**, e04812-22 (2023).
20. Townsend, E. M. *et al.* Isolation and Characterization of *Klebsiella* Phages for Phage Therapy. *PHAGE: Therapy, Applications, and Research* **2**, 26–42 (2021).
21. Ferriol-González, C. & Domingo-Calap, P. The host range of generalist and specialist phages in capsule-diverse Klebsiella hosts is driven by the evolvability of receptor-binding proteins. *PLoS Biol* **23**, e3003515 (2025).
22. Gembara, K. & Dąbrowska, K. Phage-specific antibodies. *Current Opinion in Biotechnology* **68**, 186–192 (2021).
23. Turner, J. S., Benet, Z. L. & Grigorova, I. L. Signals 1, 2 and B cell fate or: Where, when and for how long? *Immunological Reviews* **296**, 9–23 (2020).
24. Skurnik, M. *et al.* Phage therapy. *Nat Rev Methods Primers* **5**, 9 (2025).
25. Luong, T. *et al.* Ecological partitioning enables phage–antibiotic cooperation in a human Pseudomonas infection. *Nat Commun* **17**, 2615 (2026).
26. Nick, J. A. *et al.* Host and pathogen response to bacteriophage engineered against Mycobacterium abscessus lung infection. *Cell* **185**, 1860-1874.e12 (2022).
27. Hodyra-Stefaniak, K. *et al.* Natural and Induced Antibodies Against Phages in Humans: Induction Kinetics and Immunogenicity for Structural Proteins of PB1-Related Phages. *PHAGE: Therapy, Applications, and Research* **1**, 91–99 (2020).
28. Kaźmierczak, Z. *et al.* Immune Response to Therapeutic Staphylococcal Bacteriophages in Mammals: Kinetics of Induction, Immunogenic Structural Proteins, Natural and Induced Antibodies. *Front. Immunol.* **12**, 639570 (2021).
29. Wang, J. *et al.* Use of bacteriophage in the treatment of experimental animal bacteremia from imipenem-resistant Pseudomonas aeruginosa. *Int J Mol Med* **17**, 309–317 (2006).
30. Łusiak-Szelachowska, M., Międzybrodzki, R., Fortuna, W., Borysowski, J. & Górski, A. Anti-phage serum antibody responses and the outcome of phage therapy. *Folia Microbiol* **66**, 127–131 (2021).

31. Dan, J. M. *et al.* Development of Host Immune Response to Bacteriophage in a Lung Transplant Recipient on Adjunctive Phage Therapy for a Multidrug-Resistant Pneumonia. *The Journal of Infectious Diseases* **227**, 311–316 (2023).
32. Cianci, R. *et al.* Cytokines Meet Phages: A Revolutionary Pathway to Modulating Immunity and Microbial Balance. *Biomedicines* **13**, 1202 (2025).
33. Federici, S., Nobs, S. P. & Elinav, E. Phages and their potential to modulate the microbiome and immunity. *Cell Mol Immunol* **18**, 889–904 (2021).
34. Walter, N. *et al.* Hydrogel-based local delivery of bacteriophages for infection control: a systematic review of in vivo evidence. *Journal of Controlled Release* 115335 (2026) doi:10.1016/j.jconrel.2026.115335.
35. Ferry, T. *et al.* The Potential Innovative Use of Bacteriophages Within the DAC® Hydrogel to Treat Patients With Knee Megaprosthesis Infection Requiring “Debridement Antibiotics and Implant Retention” and Soft Tissue Coverage as Salvage Therapy. *Front. Med.* **7**, 342 (2020).
36. Alt, V. *et al.* Case report: Local bacteriophage therapy for fracture-related infection with polymicrobial multi-resistant bacteria: hydrogel application and postoperative phage analysis through metagenomic sequencing. *Front. Med.* **11**, 1428432 (2024).
37. Andrey, D. O. *et al.* An Emerging Clone, Klebsiellapneumoniae Carbapenemase 2–Producing K. pneumoniae Sequence Type 16, Associated With High Mortality Rates in a CC258-Endemic Setting. *Clinical Infectious Diseases* **71**, e141–e150 (2020).
38. Martins, W. M. B. S. *et al.* Effective phage cocktail to combat the rising incidence of extensively drug-resistant *Klebsiella pneumoniae* sequence type 16. *Emerging Microbes & Infections* **11**, 1015–1023 (2022).
39. Miura, K. *et al.* Development and characterization of a standardized ELISA including a reference serum on each plate to detect antibodies induced by experimental malaria vaccines. *Vaccine* **26**, 193–200 (2008).

40. Pirnay, J.-P. *et al.* Personalized bacteriophage therapy outcomes for 100 consecutive cases: a multicentre, multinational, retrospective observational study. *Nat Microbiol* **9**, 1434–1453 (2024).
41. Cano, E. J. *et al.* Phage Therapy for Limb-threatening Prosthetic Knee *Klebsiella pneumoniae* Infection: Case Report and In Vitro Characterization of Anti-biofilm Activity. *Clinical Infectious Diseases* **73**, e144–e151 (2021).
42. Eskenazi, A. *et al.* Combination of pre-adapted bacteriophage therapy and antibiotics for treatment of fracture-related infection due to pandrug-resistant Klebsiella pneumoniae. *Nat Commun* **13**, 302 (2022).
43. Kim, P. *et al.* Safety, pharmacokinetics, and pharmacodynamics of LBP-EC01, a CRISPR-Cas3-enhanced bacteriophage cocktail, in uncomplicated urinary tract infections due to Escherichia coli (ELIMINATE): the randomised, open-label, first part of a two-part phase 2 trial. *The Lancet Infectious Diseases* **24**, 1319–1332 (2024).
44. Cammuso, M. T. *et al.* First Use of Phage Therapy in Canada for the Treatment of a Life-Threatening, Multidrug-Resistant Staphylococcus epidermidis Periprosthetic Joint Infection. *Viruses* **17**, 1118 (2025).
45. Doub, J. B. *et al.* Salphage: salvage bacteriophage therapy for a recalcitrant Klebsiella pneumoniae prosthetic shoulder infection — a case report. *ActaO* **93**, 756–759 (2022).
46. Nir-Paz, R. *et al.* Successful Treatment of Antibiotic-resistant, Poly-microbial Bone Infection With Bacteriophages and Antibiotics Combination. *Clinical Infectious Diseases* **69**, 2015–2018 (2019).
47. Mora-Quilis, L. *et al.* Favorable clinical and microbiological outcomes of a war-associated prosthetic joint infection caused by Klebsiella pneumoniae treated with combined phage-colistin therapy. *International Journal of Infectious Diseases* **171**, 109079 (2026).
48. Simner, P. J. *et al.* Combination of phage therapy and cefiderocol to successfully treat *Pseudomonas aeruginosa* cranial osteomyelitis. *JAC-Antimicrobial Resistance* **4**, dlac046 (2022).

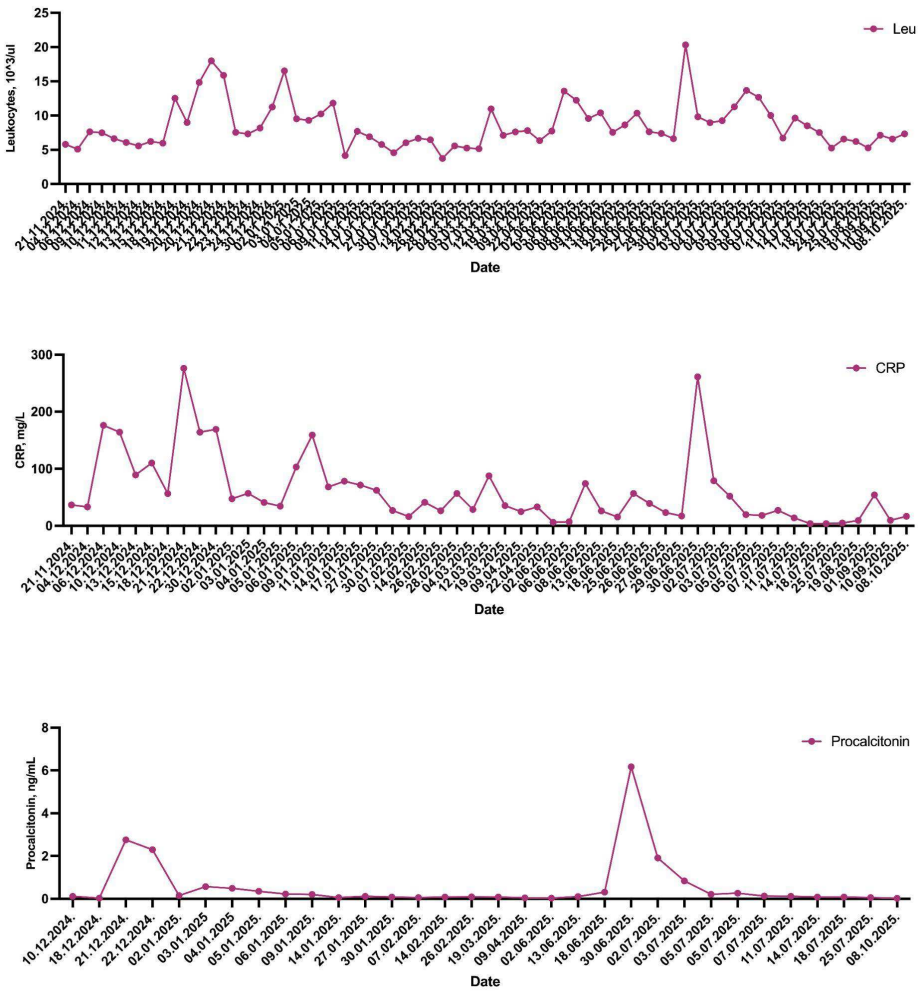
49. Yang, X. *et al.* Combined bacteriophage and antibiotic therapy for refractory peritoneal dialysis-related peritonitis caused by Klebsiella pneumoniae. *Nat Commun* **17**, 2468 (2026).
50. Hodyra-Stefaniak, K. *et al.* Bacteriophages engineered to display foreign peptides may become short-circulating phages. *Microbial Biotechnology* **12**, 730–741 (2019).
51. Hung, C.-H., Kuo, C.-F., Wang, C.-H., Wu, C.-M. & Tsao, N. Experimental Phage Therapy in Treating Klebsiella pneumoniae-Mediated Liver Abscesses and Bacteremia in Mice. *Antimicrob Agents Chemother* **55**, 1358–1365 (2011).
52. Bernabéu-Gimeno, M. *et al.* Neutralizing antibodies after nebulized phage therapy in cystic fibrosis patients. *Med* **5**, 1096-1111.e6 (2024).
53. Stepanović, S. *et al.* Quantification of biofilm in microtiter plates: overview of testing conditions and practical recommendations for assessment of biofilm production by staphylococci. *APMIS* **115**, 891–899 (2007).
54. Bouras, G. *et al.* Hybracter: Enabling Scalable, Automated, Complete and Accurate Bacterial Genome Assemblies. Preprint at https://doi.org/10.1101/2023.12.12.571215 (2023).
55. Chklovski, A., Parks, D. H., Woodcroft, B. J. & Tyson, G. W. CheckM2: a rapid, scalable and accurate tool for assessing microbial genome quality using machine learning. *Nat Methods* **20**, 1203–1212 (2023).
56. Li, W. *et al.* RefSeq: expanding the Prokaryotic Genome Annotation Pipeline reach with protein family model curation. *Nucleic Acids Research* **49**, D1020–D1028 (2021).
57. Mora-Quilis, L., Sanjuán, R. & Domingo-Calap, P. Reversible phenotypic resistance to phage infection via capsule downregulation in Klebsiella pneumoniae. *iScience* **28**, 114107 (2025).
58. Roch, M., Sierra, R., Panis, G., Martins, W. B. & Andrey, D. Synergistic activity of a KL51-depolymerase and a *Sugarlandvirus* bacteriophage against ST16 *Klebsiella pneumoniae*. *Microbiol Spectr* **13**, e02142-25 (2025).

59. SIERRA, R., ROCH, M., JAQUIER, D., ANDREY, D. The GENeva PHage (GENPH) collection against multidrug resistant Klebsiella pneumoniae. in (Guimaraes, Portugal., 2022).

Supplementary information

Supplementary Table 1. Antimicrobial susceptibility of the patient's *K. pneumoniae* isolates throughout hospital stay. Susceptibility interpreted per EUCAST breakpoints (version 14.0 and 15.0) S, susceptible; R, resistant; I, susceptible, increased exposure.

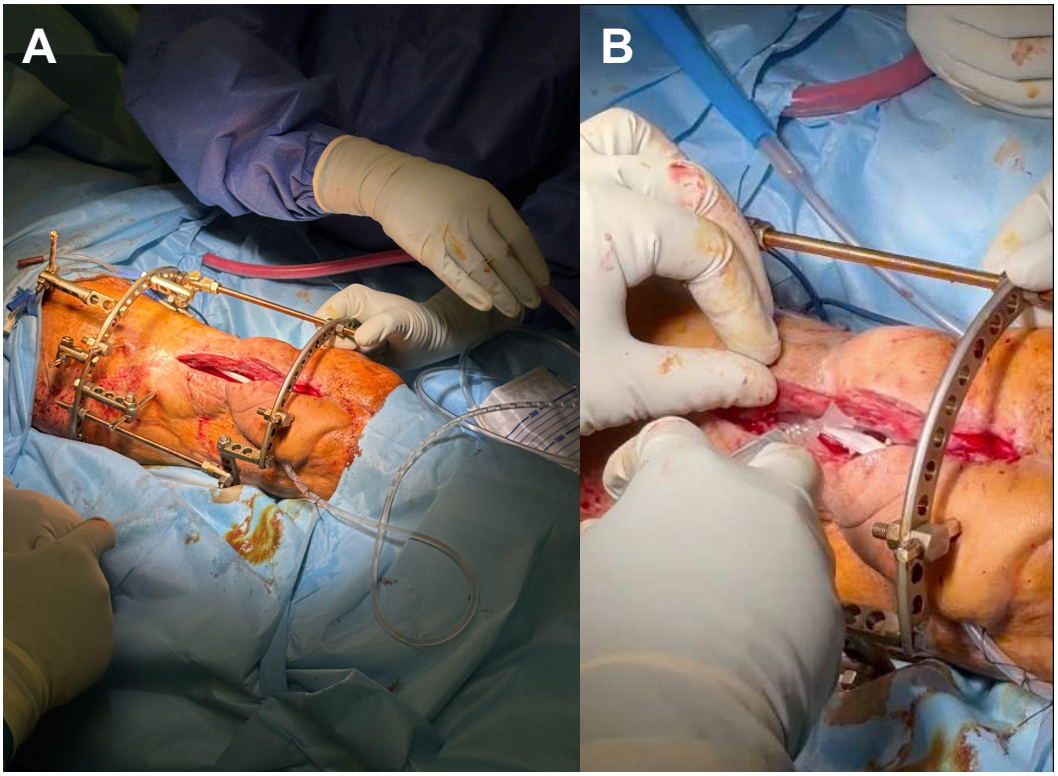
AB	14.12.2024. *K. pneumoniae* (deep soft tissue near the right knee)	14.12.2024. *K. pneumoniae* (deep soft tissue near the right knee)	18.12.2024. *K.pneumoniae* (from plate)	02.01.2025. *K.pneumoniae* (from bone)	05.06.2025. *K.pneumoniae* (surgery material - bone)	05.06.2025. *K.pneumoniae* (surgery material)
Ampicillin	R	R	R	R	-	R
Amoxicillin/ Clavulanic acid (i/v)	R	R	R	R	R	R
Amoxicillin/ Clavulanic acid (per os)	-	-	R	R	R	R
Piperacillin	-	-	-	-	-	R
Piperacillin/ Tazobactam	R	R	R	R	R	R
Cefepime	R	R	-	R	R	R
Ceftazidime	-	-	-	-	R	-
Ceftazidime/ Avibactam	S	S	S	S	S	S
Ceftolozane/ Tazobactam	-	R	-	-	-	R
Ceftriaxone	R	R	R	R	R	R
Imipenem	R	R	R	I	R	R
Meropenem	R	R	R	R	S	I
Amikacin	R	R	R	R	R	R
Gentamicin	S	R	R	S	S	S
Ciprofloxacin	R	R	R	R	R	R
Levofloxacin	-	R	-	-	-	R
Colistin	S	S	S	S	S	S
Trimethoprim/ Sulfamethoxazole	S	R	R	R	R	R



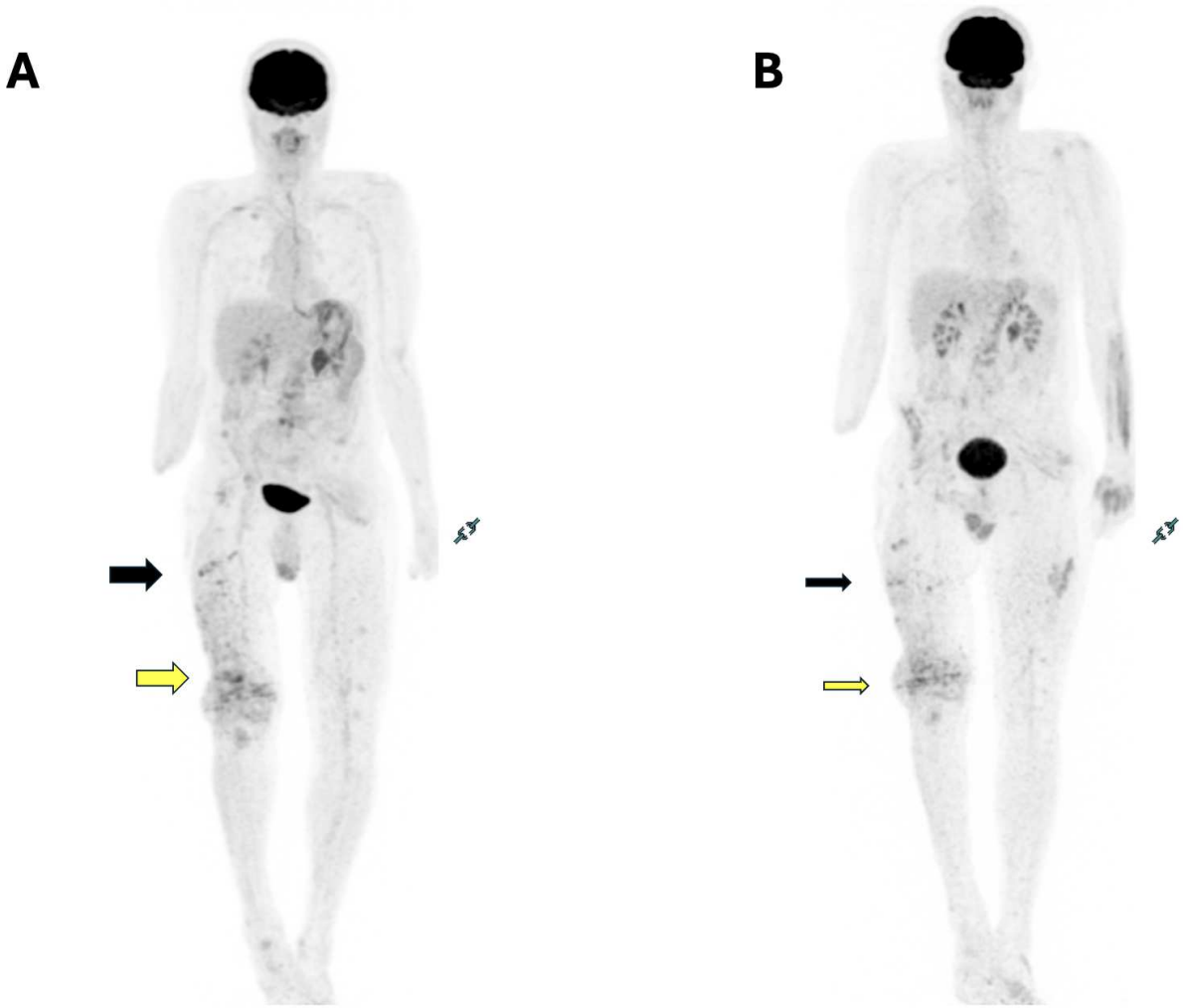
Supplementary Figure 1. Leukocyte count, CRP, and procalcitonin levels over the period of hospital stay.



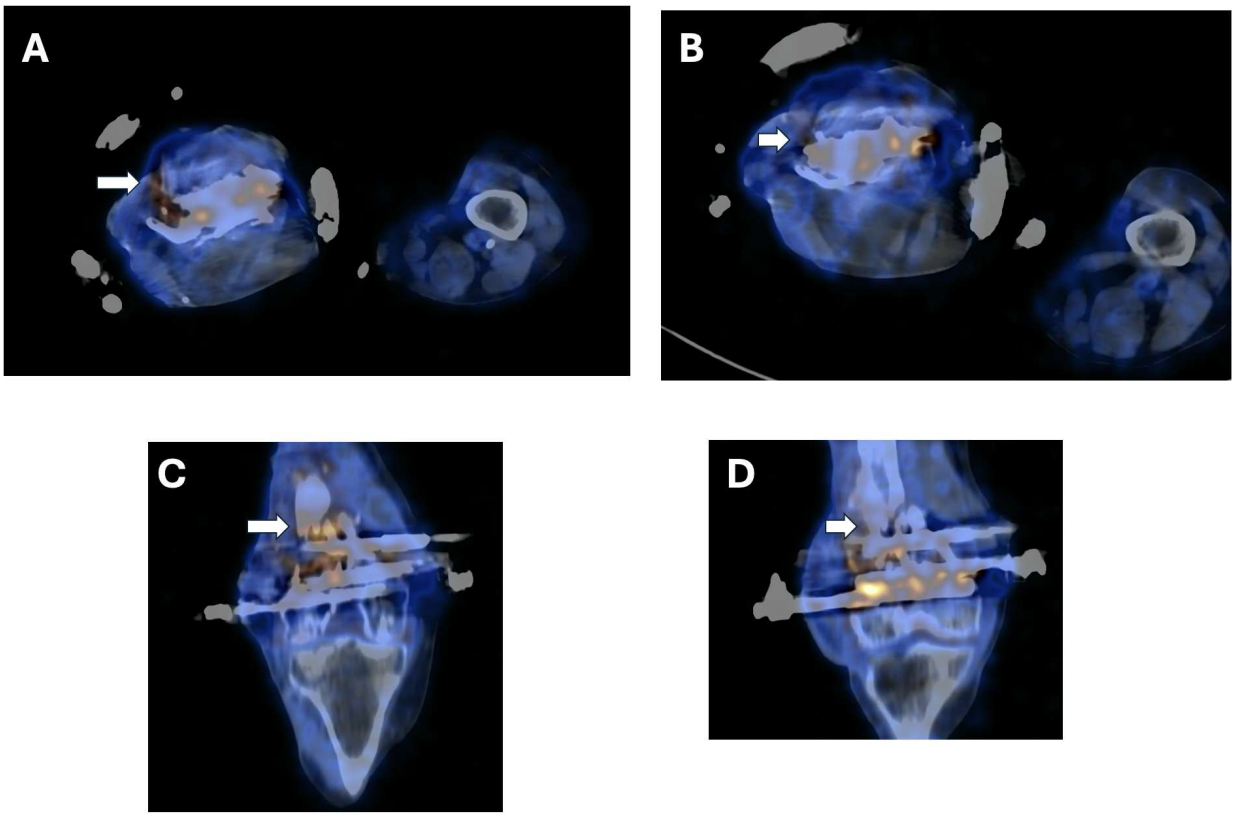
Supplementary Figure 2. Intraoperative phage preparations, including DAC hydrogel loaded with phage suspension at 10^7 PFU/mL in 0.9% NaCl in July 2025.



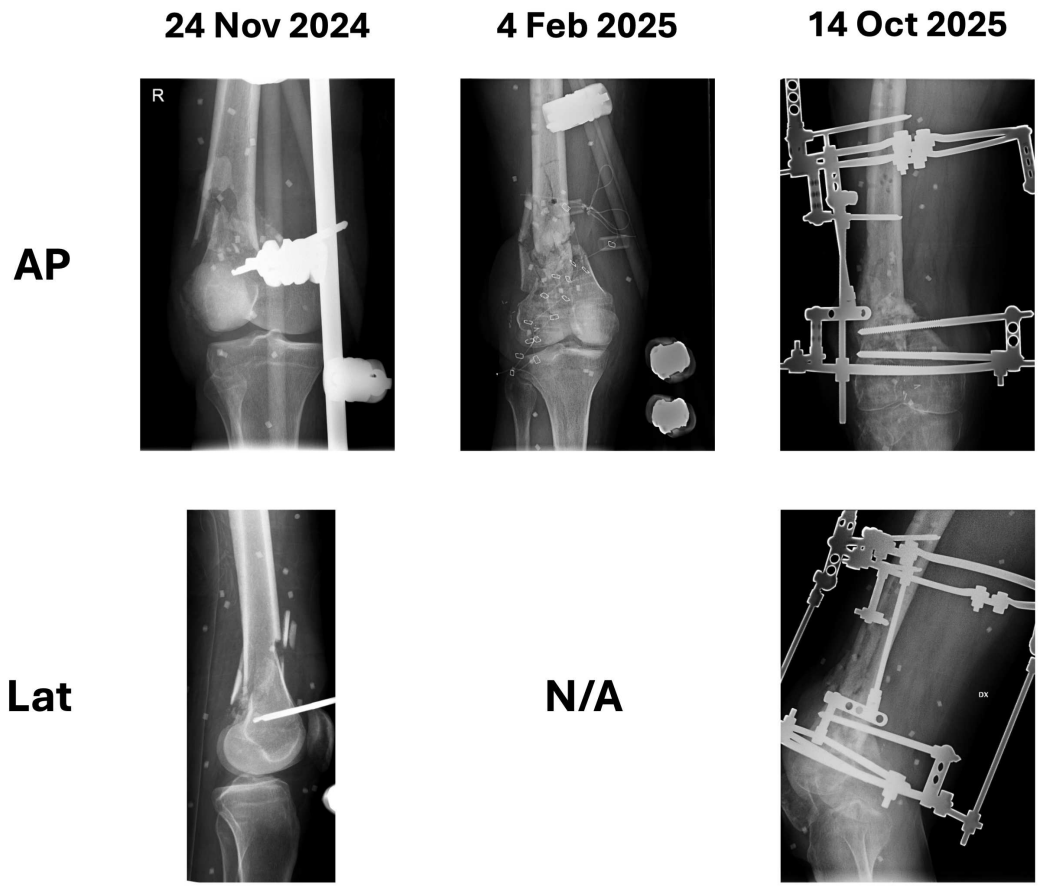
Supplementary Figure 3A and 3B. Clinical appearance of the patient's right leg during the surgery when phage treatment was initiated in July 2025. 3A - intramedullary catheter, 3B - DAC hydrogel application.



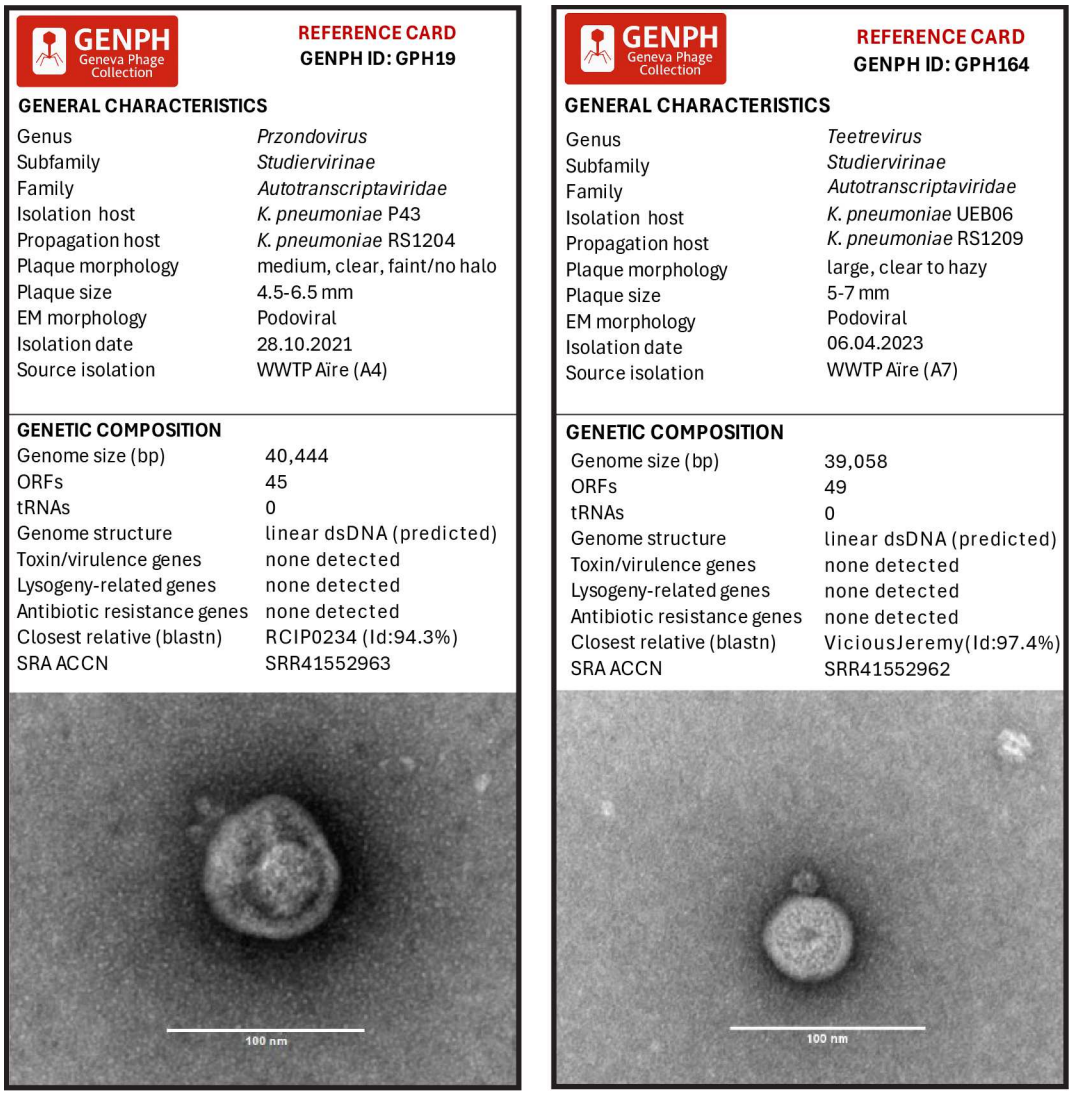
Supplementary Figure 4. Whole-body ^{18F}FDG PET maximum intensity projection images obtained before and 4 months after bacteriophage therapy in a patient with chronic osteomyelitis of the right femur with external fixation. A. Pre-treatment imaging demonstrates increased FDG uptake in the right thigh, most pronounced along the proximal fixation screw (black arrows) and around the knee joint in the region of distal screws (yellow arrows). B. Follow-up imaging shows a visually appreciable decrease in FDG uptake in the same regions (black and yellow arrows), although residual metabolic activity persists. No evidence of distant infectious spread is observed.



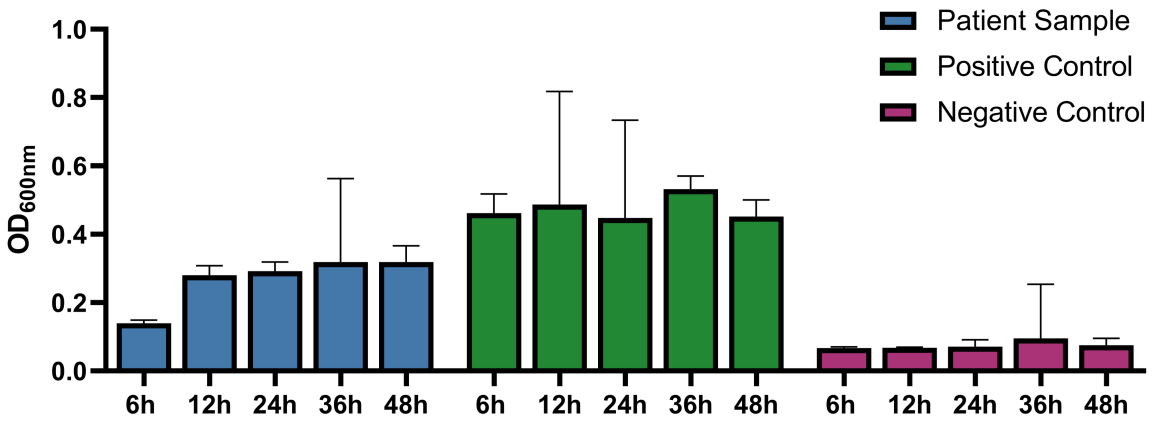
Supplementary Figure 5. FDG PET/CT of chronic osteomyelitis of the right femur with external fixation. Axial (A, B) and coronal (C, D) fused images obtained before and after bacteriophage therapy. (A, C) Pre-treatment imaging demonstrates heterogeneous FDG uptake in the right thigh, most pronounced along the fixation hardware and at the non-union fracture site, particularly around the distal fixation screw near the knee joint (arrows), suspicious for active infection in the post-surgical setting. (B, D) Follow-up imaging shows a visually appreciable reduction in FDG uptake in the same region (arrows), although residual metabolic activity persists, consistent with partial metabolic response. Sustained clinical improvement without recurrence of infection was observed.



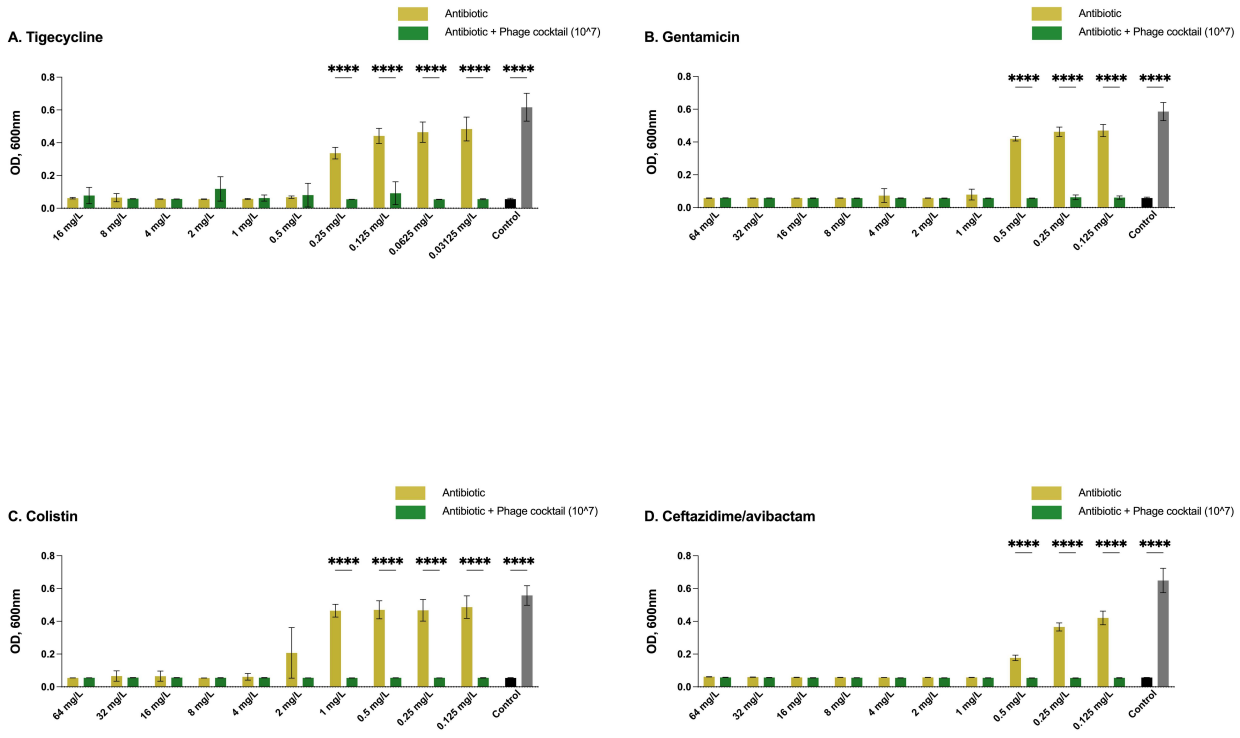
Supplementary Figure 6. Radiographic series of the right distal femur. Anteroposterior (AP) and lateral radiographs on 24 Nov 2024, 4 Feb 2025, and 14 Oct 2025 showing a multifragmentary distal femoral fracture with external fixation. Multiple metallic fragments are present in the soft tissues. The lateral view from 4 Feb 2025 was not available.



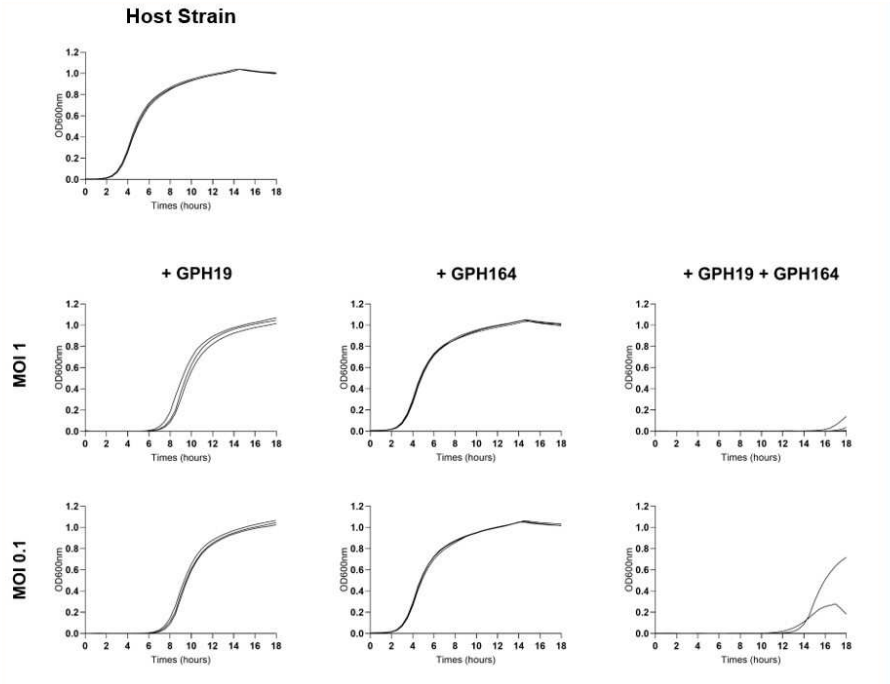
Supplementary Figure 7. GENPH reference cards for the therapeutic phages GPH19 and GPH164. Reference cards for the GENPH Collection summarizing the genomic and biological characteristics of the two lytic phages used in this study. The cards include phage taxonomy, genome features, predicted coding sequences, and quality-control metrics relevant for therapeutic application. GPH19 and GPH164 were selected as a dual-phage combination based on their complementary activity against KL107-producing ST512 *K. pneumoniae* isolates.



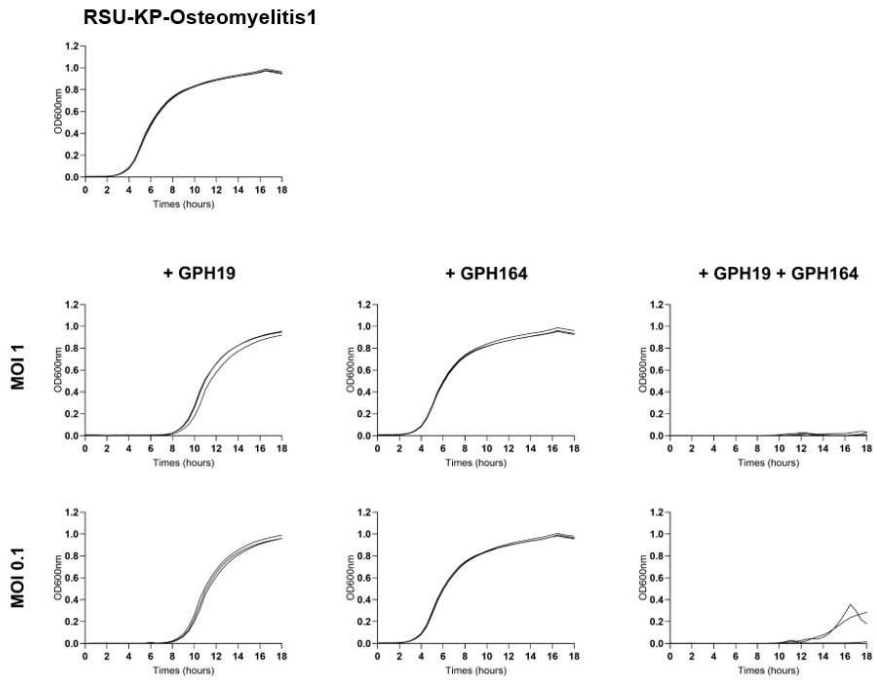
Supplementary Figure 8. Time-dependent biofilm formation of the patient-derived *K. pneumoniae* isolate compared to a positive and negative control.



Supplementary Figure 9. MIC of antibiotics in combination with a dual-phage combination (GPH19 and GPH164) (**** - p<0.0001).



Supplementary Figure 10. GPH19 and GPH164 interaction with the original encapsulated host strain. Growth curves of the encapsulated host strain exposed to both phages separately and in combination at MOI 1 and MOI 0.1. Individual phages were followed by bacterial outgrowth, whereas the dual-phage combination showed the most sustained inhibition. Bacterial growth was monitored by optical density every 30 min for 18 h. Data are shown as mean ± SD from biological triplicates.



Supplementary Figure 11. Activity of the DPC against the patient-derived *K. pneumoniae* strain RSU-KP-Osteomyelitis1. Growth curves of the patient-derived ST512 strain RSU-KP-Osteomyelitis1 cultured in cation-adjusted Mueller–Hinton broth in the absence of phage (control, top), in the presence of individual phages alone, or in the presence of the DPC. Conditions are shown at both MOI 1 and MOI 0.1. Bacterial growth was monitored by optical density measurements every 30 min for 18 h in a plate reader. Data are shown as mean ± SD from biological triplicates.

Supplementary Note 1. Genomic features of the bacterial isolate.

Trimmed paired-end Illumina read dataset (SRR41443481) for the strain isolated on 5 June 2025 from surgical material collected during the operation comprised ~140 Mbp of data split into 386,964 read pairs of up to 250 base pairs in length, with an average read length of ~181 bp, whereas the combined trimmed long-read Nanopore datasets (SRR41443480) comprised ~178 Mbp of data split into 35,968 reads with an average length of ~4,952 bp. Hybrid de novo assembly of the trimmed read datasets using Hybracter has resulted in a 5,884,927 bp assembly comprising 6 contigs (JCFYWV000000000) representing complete circularized replicons, namely 5,371,657 bp chromosomes with an average depth of 27x and five putative plasmids of 250,605, 190,702, 53,292, 15,708, 2963 bp in length, respectively. Quality assessment of the resulting de novo assembly using CheckM2 Neural Network (Specific Model) estimated general and specific completeness as 98.57% and 100.0%, respectively, while the contamination was estimated at 0.42%. Kleborate predicted the isolate to represent K. pneumoniae ST512 based on the respective MLST scheme, with a resistance

score of 2 and a virulence score of 0. The capsule locus was most reminiscent of KL107 according to the Kaptive analysis (K locus identity 99.86%).